

Bound-electron self-energy calculations in Feynman and Coulomb gauges: detailed analysis

M. A. Reiter,¹ E. O. Lazarev,² D. A. Glazov,^{2,3} A. V. Malyshev,^{1,3} and A. V. Volotka²

¹*Department of Physics, St. Petersburg State University,
Universitetskaya nab. 7/9, 199034 St. Petersburg, Russia*

²*School of Physics and Engineering, ITMO University,
Kronverkskiy pr. 49, 197101 St. Petersburg, Russia*

³*Petersburg Nuclear Physics Institute named by B.P. Konstantinov of NRC “Kurchatov Institute”,
Orlova roscha 1, 188300 Gatchina, Leningrad region, Russia*

The energy correction associated with the self-energy diagram is the leading (in magnitude) and fundamental (in significance) contribution to the Lamb shift in highly charged ions. Conventional approaches to this correction rely on partial-wave expansions, which is a stumbling block limiting accuracy. To elucidate the issue, we perform a comprehensive comparative analysis of partial-wave-expansion convergence between two gauges: Feynman and Coulomb. Some tricks for improving the convergence are discussed as well.

I. INTRODUCTION

Quantum electrodynamics (QED) effects are indispensable for the accurate theoretical description of various atomic systems. To account for relativistic effects, the corresponding calculations are to be performed non-perturbatively in the nuclear-strength parameter αZ (α is the fine-structure constant and Z is the nuclear charge). In the present work, we employ the related formalism known as the Furry picture of QED [1]. We note that the corresponding approach is relevant not only for highly charged ions [2–9], but also finds application in the case of light systems including the hydrogen atom, see, e.g., Refs. [10–13]. An alternative, and in some sense complementary, nonrelativistic QED approach [14], primarily applicable to low- Z systems, is beyond the scope of this paper. One of the leading QED corrections to energy levels originates from the one-electron self-energy (SE) diagram, shown in Fig. 1.

However, high-precision evaluation of the corresponding contribution holds significance not only for studying the Lamb shift and transition energies in hydrogen-like ions and other few-electron systems [15–22] (for related theory, see, e.g., Refs. [23–28]), but also for investigating a wide range of atomic properties. Accurate calculations of the SE contribution is a cornerstone in the *ab initio* treatment of the one-electron QED corrections to the g factor [29, 30], hyperfine structure [31–34], quadratic Zeeman splitting [35], nuclear-magnetic shielding [36, 37], E1 [38] and M1 [39] transition amplitudes. The SE contribution also plays an important role in the treatment of various many-electron QED effects, see, e.g., [40–44] and references therein. In all these applications it is often necessary to calculate off-diagonal matrix elements of the SE operator. However, the one-electron (diagonal) SE contribution is the simplest example that one can and should use to probe different methods and numerical approaches.

Within the Furry-picture formalism, an issue of representing the bound-electron propagator in calculations naturally arises. Unlike the free-electron propagator, the propagator in the presence of external field generally does not have a closed-form expression. However, when the spherical symmetry is present, as is the case of atomic electrons, the partial-wave (PW) expansion helps to construct the propagator. With this in mind, we use two state-of-the-art approaches: the Green’s function (GF) method [45–48], and the finite-basis-set (FBS) method [49–52].

Within the first approach, the bound-electron propagator is represented in terms of the Dirac-equation solutions bounded at infinity and at origin. For the point-nucleus Coulomb potential, the corresponding solutions are expressed analytically via the Whittaker functions [53]. For more realistic models of nuclear-charge distribution, e.g., the Fermi model, or other spherically symmetric potentials, e.g., some local screening potentials, these solutions can be found numerically. This approach enables one to perform calculations with a high numerical accuracy when large numerical cancellations occur or when the PW expansion does not converge rapidly. Note that the Green’s function, considered as a function of any of its radial arguments, is discontinuous, when the arguments coincide. Therefore, obtaining accurate results for the matrix elements of the Green’s function requires special care.

Within the second approach, the electron Green’s function is represented using the FBS’s. The basis sets for the Dirac equation can be constructed, e.g., from the B splines [52, 54, 55], Sturm orbitals [50, 51, 56] or Gaussians [57, 58]. The corresponding numerical procedures can easily incorporate any spherically symmetric potential. Moreover, for systems that do not possess spherical symmetry, the FBSs can also be readily prepared [59–61]. The advantage of this method is that it allows one to easily separate out and exclude, if necessary, the contribution of a specific bound state to the Green’s function. Note also that this method provides an approximation to the Green’s function, which is a continuous function of the radial arguments. Nevertheless, the basis-set method has some important drawbacks when compared to the GF approach. Because of an additional parameter, the number of basis functions N , the

obtained results should be extrapolated to $N \rightarrow \infty$. Typically, this sets a limit on the computational accuracy. Furthermore, the number of partial waves, usually accessible in practical calculations by means of the FBS method, is limited and smaller than that in the Green's function method [48]. In this paper, we use the FBS method with the basis obtained from B splines within the dual-kinetic-balance (DKB) approach [52]. The latter method eliminates the so-called spurious states and establishes the correct asymptotics of wave functions in the non-relativistic limit. The effectiveness of this basis for calculating the SE correction has been demonstrated, e.g., in Ref. [52] for the Coulomb potential and in Ref. [62] for local screening potentials.

The SE diagram contains ultraviolet (UV) divergences. In the present work, these divergences are renormalized using the conventional approach based on the potential expansion of the bound-electron propagator [63]. Within this expansion, three contributions naturally arise: zero-, one-, and many-potential terms. Only the zero- and one-potential terms, which correspond to the first and second terms of the potential expansion, are UV divergent. They are treated separately in momentum space together with the mass counterterm. The remaining many-potential term is considered in coordinate space using the PW expansion. The truncation of this expansion and subsequent estimation of the residual is generally the main source of numerical uncertainty of the results.

The total SE contribution is gauge invariant, unlike the individual terms of its potential expansion. It is therefore intriguing to compare the magnitude of these terms in different gauges of the photon propagator. Starting from the pioneering works [45, 46], the SE correction is calculated predominantly in the Feynman gauge, see, e.g., Refs. [46, 64–68] and references therein. In the Coulomb gauge, similar calculations were carried out in Refs. [69, 70]. These works suggest that the many-potential contribution is significantly smaller in the Coulomb gauge. However, a smaller absolute value does not necessarily imply better convergence of the PW expansion. Therefore, a thorough comparative analysis of the many-potential contributions in both gauges is in demand. Note that other covariant gauges, aside from the Feynman one, can also be applied to the SE calculations. For example, the Fried-Yennie gauge [71] was also considered in Ref. [70]. In the present work, however, we restrict our consideration only to the Feynman and Coulomb gauges.

Another important issue in the SE calculations is to somehow accelerate the convergence of PW expansions mentioned above. It is reasonable to assume that the poor convergence of the many-potential contribution is due to the leading term of its potential expansion. Therefore, the natural first step is to additionally subtract the two-potential term, which should improve the convergence of the remainder. The subtracted term has to be evaluated separately with high precision within some alternative method. In the following, we will refer to this approach as the two-potential scheme. It should be noted, however, that the direct calculation of the two-potential term in momentum space in a closed form, i.e., not resorting to the PW expansion, turns out to be a challenging problem [33, 72].

Another convergence-acceleration approach, hereafter referred to as the Sapirstein-Cheng (SC) scheme, was proposed recently in Ref. [73]. Within the framework of this promising scheme, the quasi-two-potential contribution, which is an approximation to the two-potential term, is subtracted from the many-potential term instead. In contrast to the exact two-potential term, its quasi-two-potential counterpart can be easily calculated in momentum space. For the point-nucleus case, calculations of the SE correction using this acceleration scheme have been performed in Ref. [70] for different gauges. However, the case of an extended nucleus is also worth examining.

Yet another convergence-acceleration approach was developed earlier for the SE contribution to the Lamb shift in Ref. [74]. We refer to it as the Yerokhin, Pachucki, and Shabaev (YPS) scheme. This scheme also improves the convergence by subtracting an approximation to the many-potential contribution, that can be calculated in a closed form. The YPS scheme was initially developed for the calculations in the Feynman gauge, and was later generalized to the Coulomb gauge in Ref. [70]. Judging by the results of the latter paper, it is an extremely powerful scheme, however, it is difficult to generalize it to more complex diagrams, unlike other convergence-acceleration approaches. For instance, the two-potential scheme has recently been applied in the QED calculations of the quadratic Zeeman effect [35], and some modifications of the SC scheme have been applied to the calculations of the two-electron SE [75] and two-loop SE [12, 76] contributions. For this reason, we do not consider the YPS scheme in the current study.

Thus we thoroughly examine the application of several different schemes to the SE calculations in both the Coulomb and Feynman gauges. We conduct an independent of Ref. [70] analysis, consider in details the issue of the PW-expansion convergence, evaluate the SE correction for finite-size nuclei, and collect the necessary formulas in a convenient form that allow one to make the corresponding calculations.

Throughout this article the relativistic units ($\hbar = c = 1$) and the Heaviside charge unit ($\alpha = e^2/(4\pi), e < 0$) are used. We use roman style (p) for four-vectors, bold style (\mathbf{p}) for space vectors, and italic style (p) for scalars.

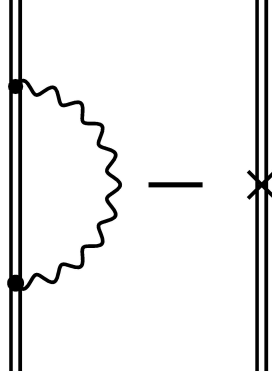


Figure 1. Self-energy diagram with the related mass counterterm. The double line indicates the electron propagator in the external field of the nucleus, the wavy line denotes the photon propagator, and the cross stands for the mass counterterm.

II. SELF-ENERGY CONTRIBUTION

A. Basic formalism

Within the framework of the Furry picture, the description of a bound electron starts with the Dirac equation:

$$[-i(\boldsymbol{\alpha} \cdot \nabla) + \beta m_e + V(\mathbf{r})] |a\rangle = \varepsilon_a |a\rangle, \quad (1)$$

where $|a\rangle$ and ε_a are the Dirac wave function and relativistic energy, $\boldsymbol{\alpha}$ and β are the Dirac matrices, $V(\mathbf{r})$ is the binding potential, which is a function of the position vector \mathbf{r} . In the following, we consider only hydrogen-like ions where the binding potential is spherically symmetric, $V(\mathbf{r}) = V(r)$, $r = |\mathbf{r}|$. Then, the solution of Eq. (1) can be represented in the form:

$$|a\rangle \leftrightarrow \psi_a(\mathbf{r}) = \begin{pmatrix} g_a(r) \chi_{\kappa_a m_a}(\hat{\mathbf{r}}) \\ i f_a(r) \chi_{-\kappa_a m_a}(\hat{\mathbf{r}}) \end{pmatrix}, \quad (2)$$

where $g_a(r)$ and $f_a(r)$ are the large and small radial components, $\chi_{\kappa_a m_a}(\hat{\mathbf{r}})$ is the spin-angular spinor, $\hat{\mathbf{r}} = \mathbf{r}/r$, $\kappa_a = (j_a + 1/2)(-1)^{j_a + l_a + 1/2}$ is the Dirac angular quantum number, l_a is the spatial parity, and m_a is the projection of the total angular momentum $j_a = |\kappa_a| - 1/2$. The radial wave functions of the bound-electron state are characterized by κ_a and the radial quantum number n_{r_a} : $g_a(r) = g_{n_{r_a} \kappa_a}(r)$, $f_a(r) = f_{n_{r_a} \kappa_a}(r)$.

The energy shift $\Delta\varepsilon_a$ of the bound state $|a\rangle$ due to the first-order self-energy correction, which is graphically represented in Fig. 1, is given by the real part of the following expression [2]:

$$\begin{aligned} \Delta\varepsilon_a = & 2i\alpha \int_{-\infty}^{\infty} d\omega \int d^3\mathbf{r}_1 d^3\mathbf{r}_2 \psi_a^\dagger(\mathbf{r}_1) \alpha^\mu \\ & \times G(\varepsilon_a - \omega, \mathbf{r}_1, \mathbf{r}_2) \alpha^\nu \psi_a(\mathbf{r}_2) D_{\mu\nu}(\omega, \mathbf{r}_{12}) \\ & - \delta m \int d^3\mathbf{r} \psi_a^\dagger(\mathbf{r}) \beta \psi_a(\mathbf{r}), \end{aligned} \quad (3)$$

where $\mathbf{r}_{12} = \mathbf{r}_1 - \mathbf{r}_2$, $D_{\mu\nu}(\omega, \mathbf{r}_{12})$ is the photon propagator, $\alpha^\mu = (1, \boldsymbol{\alpha})$, $G(\varepsilon, \mathbf{r}_1, \mathbf{r}_2)$ is the bound-electron Green's function, and δm is the mass counterterm. Let us define the gauge-dependent operator $I(\omega, \mathbf{r}_1, \mathbf{r}_2)$ according to

$$I(\omega, \mathbf{r}_1, \mathbf{r}_2) = e^2 \alpha^\nu \alpha^\mu D_{\mu\nu}(\omega, \mathbf{r}_{12}). \quad (4)$$

In the Feynman and Coulomb gauges, this operator takes the forms I_F and I_C , respectively,

$$I_F(\omega, \mathbf{r}_1, \mathbf{r}_2) = \alpha [1 - (\boldsymbol{\alpha}_1 \cdot \boldsymbol{\alpha}_2)] \frac{e^{i\omega r_{12}}}{r_{12}}, \quad (5)$$

$$I_C(\omega, \mathbf{r}_1, \mathbf{r}_2) = \alpha \left[\frac{1}{r_{12}} - (\boldsymbol{\alpha}_1 \cdot \boldsymbol{\alpha}_2) \frac{e^{i\omega r_{12}}}{r_{12}} + (\boldsymbol{\alpha}_1 \cdot \nabla_1)(\boldsymbol{\alpha}_2 \cdot \nabla_2) \frac{e^{i\omega r_{12}} - 1}{\omega^2 r_{12}} \right], \quad (6)$$

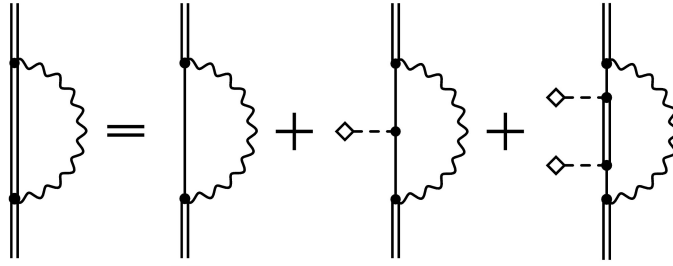


Figure 2. Potential expansion of the self-energy diagram. The dashed line ended by a rhombus denotes the interaction with the binding potential. The single line denotes the free-electron propagator. The mass counterterm is not shown.

where $r_{12} = |\mathbf{r}_{12}|$, $\hat{\omega} = \sqrt{\omega^2 + i0}$, and the branch of the square root is fixed with the condition $\text{Im} \sqrt{\omega^2 + i0} > 0$.

The bound-electron propagator G can be expressed using the spectral representation,

$$G(\omega, \mathbf{r}_1, \mathbf{r}_2) = \sum_n \frac{\psi_n(\mathbf{r}_1)\psi_n^\dagger(\mathbf{r}_2)}{\omega - \varepsilon_n(1 - i0)}, \quad (7)$$

where the summation runs over the complete Dirac spectrum. In shortened form, the formula (7) can be written as follows:

$$G(\omega) = \sum_n \frac{|n\rangle\langle n|}{\omega - \varepsilon_n^-}, \quad (8)$$

where the notation $\varepsilon_n^- = \varepsilon_n(1 - i0)$ was introduced. Then, the energy shift (3) can be expressed as:

$$\Delta\varepsilon_a = \langle a|\gamma^0[\Sigma(\varepsilon_a) - \delta m]|a\rangle, \quad (9)$$

where $\gamma^0 \equiv \beta$ and the diagonal matrix element of the one-loop self-energy operator $\Sigma(E)$ is given by:

$$\langle a|\gamma^0\Sigma(E)|a\rangle = \frac{i}{2\pi} \int_{-\infty}^{\infty} d\omega \sum_n \frac{\langle an|I(\omega)|na\rangle}{E - \omega - \varepsilon_n^-}. \quad (10)$$

The expression (10) contains the UV divergences. To properly treat them, we expand the bound-electron propagator G in powers of the binding potential V [77]. The potential expansion can be conveniently written as:

$$\begin{aligned} G(\omega) &= \sum_f \frac{|f\rangle\langle f|}{\omega - \varepsilon_f^-} + \sum_{f_1, f_2} \frac{|f_1\rangle\langle f_1|V|f_2\rangle\langle f_2|}{(\omega - \varepsilon_{f_1}^-)(\omega - \varepsilon_{f_2}^-)} + \\ &+ \sum_{f_1, f_2, n} \frac{|f_1\rangle\langle f_1|V|n\rangle\langle n|V|f_2\rangle\langle f_2|}{(\omega - \varepsilon_{f_1}^-)(\omega - \varepsilon_n^-)(\omega - \varepsilon_{f_2}^-)}, \end{aligned} \quad (11)$$

where the states $|n\rangle$ correspond to the bound-electron spectrum, the states $|f\rangle$, $|f_1\rangle$, and $|f_2\rangle$ correspond to the free-electron spectrum, and the last term is expressed via the bound-electron Green's function $G(\omega)$ itself and encompasses an infinite number of terms corresponding to the two or more interactions with the nucleus. As before, all summations in Eq. (11), are carried out over the complete spectra for the corresponding Dirac Hamiltonians. Substituting the potential expansion (11) into Eq. (10) results in the SE diagram being split into three contributions, as shown graphically in Fig. 2. These contributions are commonly referred to as the zero-, one-, and many-potential terms. The zero- and one-potential terms diverge, whereas the many-potential term is UV finite. The UV-divergent terms have to be renormalized along with the mass counterterm. For this aim, they are considered in momentum space, and the dimensional regularization is applied to isolate and eliminate the UV divergences. This renormalization procedure yields the UV-finite contributions $\Delta\varepsilon_a^{0p}$ and $\Delta\varepsilon_a^{1p}$ to the Lamb shift. The many-potential term $\Delta\varepsilon_a^{\text{MP}}$ is calculated in the coordinate space. Finally, the SE correction to energy levels is expressed as the gauge-invariant sum of three contributions:

$$\Delta\varepsilon_a = \Delta\varepsilon_a^{0p} + \Delta\varepsilon_a^{1p} + \Delta\varepsilon_a^{\text{MP}}. \quad (12)$$

In the following subsections we consider in detail these terms and some specific methods to improve the convergence of the partial-wave expansion in the many-potential part.

B. Zero- and one-potential terms

The Fourier transform of the wave function (2), which solves the Dirac equation (1) in a spherically-symmetric potential, reads as:

$$\psi_a(\mathbf{p}) = \int d^3\mathbf{r} e^{-i(\mathbf{p}\cdot\mathbf{r})} \psi_a(\mathbf{r}) = i^{-l_a} \begin{pmatrix} \tilde{g}_a(p) \chi_{\kappa_a m_a}(\hat{\mathbf{p}}) \\ \tilde{f}_a(p) \chi_{-\kappa_a m_a}(\hat{\mathbf{p}}) \end{pmatrix}, \quad (13)$$

where $\hat{\mathbf{p}} = \mathbf{p}/p$, $l_a = |\kappa_a + 1/2| - 1/2$, and for the bound state $\tilde{g}_a(p) = \tilde{g}_{n_r a \kappa_a}(p)$ and $\tilde{f}_a(p) = \tilde{f}_{n_r a \kappa_a}(p)$. In the point-nucleus case, there are analytical expressions for $\tilde{g}_a(p)$ and $\tilde{f}_a(p)$, which can be found, e.g., Ref. [2]. For an arbitrary potential, they can be obtained numerically according to:

$$\tilde{g}_a(p) = 4\pi \int_0^\infty dr r^2 j_{l_a}(pr) g_a(r), \quad (14)$$

$$\tilde{f}_a(p) = -4\pi \frac{\kappa_a}{|\kappa_a|} \int_0^\infty dr r^2 j_{2j_a - l_a}(pr) f_a(r), \quad (15)$$

where j_l is the spherical Bessel function of the first kind.

The zero-potential term is expressed as:

$$\Delta\varepsilon_a^{0p} = \int \frac{d^3\mathbf{p}}{(2\pi)^3} \psi_a^\dagger(\mathbf{p}) \gamma^0 \Sigma_R^{(0)}(\mathbf{p}) \psi_a(\mathbf{p}), \quad (16)$$

where $\Sigma_R^{(0)}$ is the renormalized self-energy operator in free-particle QED and $\mathbf{p} = (\varepsilon_a, \mathbf{p})$. The explicit form of the operator $\Sigma_R^{(0)}$ is presented in Appendix A in Eq. (A6) with the gauge-dependent coefficients a , b , and c defined in Eqs. (A7) and (A10). After substituting Eqs. (A6) and (13) into Eq. (16), it becomes possible to analytically perform the integration over the angular variables using the relation $(\boldsymbol{\sigma} \cdot \hat{\mathbf{p}}) \chi_{\kappa\mu}(\hat{\mathbf{p}}) = -\chi_{-\kappa\mu}(\hat{\mathbf{p}})$ and the orthonormality condition for the spin-angular spinors. This results in an expression for the zero-potential contribution, which is convenient for numerical calculations:

$$\Delta\varepsilon_a^{0p} = \frac{\alpha}{4\pi} \int_0^\infty \frac{p^2 dp}{(2\pi)^3} \{a(\varepsilon_a, p)[\tilde{g}_a^2 - \tilde{f}_a^2] + b(\varepsilon_a, p)[\varepsilon_a(\tilde{g}_a^2 + \tilde{f}_a^2) + 2p\tilde{g}_a\tilde{f}_a] + c(\varepsilon_a, p)[\tilde{g}_a^2 + \tilde{f}_a^2]\}, \quad (17)$$

where the dependence of \tilde{g}_a and \tilde{f}_a on p is omitted for brevity.

The one-potential term is expressed as:

$$\Delta\varepsilon_a^{1p} = \int \frac{d^3\mathbf{p}' d^3\mathbf{p}}{(2\pi)^6} \psi_a^\dagger(\mathbf{p}') \gamma^0 \Gamma_R^{(0)}(\mathbf{p}', \mathbf{p}) \tilde{V}(|\mathbf{p}' - \mathbf{p}|) \psi_a(\mathbf{p}), \quad (18)$$

where $\Gamma_R^{(0)}$ is the renormalized free-particle vertex function, the explicit form of which with the gauge-dependent coefficients A - G_2 is given in the Appendix B in Eq. (B3), \tilde{V} is the Fourier transform of the binding potential, and $\mathbf{p} = (\varepsilon_a, \mathbf{p})$ and $\mathbf{p}' = (\varepsilon_a, \mathbf{p}')$. In this case, the angular integration can be performed using the identity:

$$\frac{1}{2j+1} \sum_m \chi_{\kappa m}^\dagger(\hat{\mathbf{p}}') \chi_{\kappa m}(\hat{\mathbf{p}}) = \frac{1}{4\pi} P_l(z), \quad (19)$$

where z is the cosine of the angle between the vectors \mathbf{p} and \mathbf{p}' , namely, $z = (\hat{\mathbf{p}} \cdot \hat{\mathbf{p}}')$, and P_l is the Legendre polynomial. The final expression for the one-potential term reads as

$$\Delta\varepsilon_a^{1p} = \frac{\alpha}{2(2\pi)^6} \int_0^\infty p'^2 dp' \int_0^\infty p^2 dp \int_{-1}^1 dz \tilde{V}(q) \{X_1 P_{l_a}(z) + X_2 P_{2j_a - l_a}(z)\}, \quad (20)$$

where $q^2 = p^2 + p'^2 - 2pp'z$. The coefficients X_1 and X_2 are defined as:

$$X_1 = A\tilde{g}'_a\tilde{g}_a + \varepsilon_a(B_1 + B_2)K'_1\tilde{g}_a + \varepsilon_a(C_1 + C_2)\tilde{g}'_a K_1 \\ + DK_1 K'_1 + \varepsilon_a(H_1 + H_2)\tilde{g}'_a\tilde{g}_a + G_1 K'_1\tilde{g}_a + G_2\tilde{g}'_a K_1, \quad (21)$$

$$X_2 = A\tilde{f}'_a\tilde{f}_a + \varepsilon_a(B_1 + B_2)K'_2\tilde{f}_a + \varepsilon_a(C_1 + C_2)\tilde{f}'_a K_2 \\ + DK_2 K'_2 - \varepsilon_a(H_1 + H_2)\tilde{f}'_a\tilde{f}_a - G_1 K'_2\tilde{f}_a - G_2\tilde{f}'_a K_2, \quad (22)$$

where

$$K_1 = \varepsilon_a \tilde{g}_a + p \tilde{f}_a, \quad K_1' = \varepsilon_a \tilde{g}'_a + p' \tilde{f}'_a, \quad K_2 = \varepsilon_a \tilde{f}_a + p \tilde{g}_a, \quad K_2' = \varepsilon_a \tilde{f}'_a + p' \tilde{g}'_a. \quad (23)$$

For brevity, the dependence of wave functions on p and p' is omitted. For the functions of p' , an additional prime is added. Thus, the shorthand notations are $\tilde{g}_a = \tilde{g}_a(p)$, $\tilde{f}_a = \tilde{f}_a(p)$, $\tilde{g}'_a = \tilde{g}_a(p')$, and $\tilde{f}'_a = \tilde{f}_a(p')$.

C. Many-potential term

As noted above, the remaining many-potential contribution is calculated in coordinate space using the PW expansion. Therefore, let us start with the PW expansion of the bound-electron propagator (7), inspired by the explicit form of the Dirac-equation solution (2):

$$G(\omega, \mathbf{r}_1, \mathbf{r}_2) = \sum_{\kappa_n} \begin{pmatrix} G_{\kappa_n}^{11}(\omega, r_1, r_2) \pi_{\kappa_n}^{++}(\hat{\mathbf{r}}_1, \hat{\mathbf{r}}_2) & -i G_{\kappa_n}^{12}(\omega, r_1, r_2) \pi_{\kappa_n}^{+-}(\hat{\mathbf{r}}_1, \hat{\mathbf{r}}_2) \\ i G_{\kappa_n}^{21}(\omega, r_1, r_2) \pi_{\kappa_n}^{-+}(\hat{\mathbf{r}}_1, \hat{\mathbf{r}}_2) & G_{\kappa_n}^{22}(\omega, r_1, r_2) \pi_{\kappa_n}^{--}(\hat{\mathbf{r}}_1, \hat{\mathbf{r}}_2) \end{pmatrix}, \quad (24)$$

where $\pi^{\pm\pm}(\hat{\mathbf{r}}_1, \hat{\mathbf{r}}_2) = \sum_{m_n} \chi_{\pm\kappa_n m_n}(\hat{\mathbf{r}}_1) \chi_{\pm\kappa_n m_n}^\dagger(\hat{\mathbf{r}}_2)$ and the components of the radial Green's function $G_{\kappa_n}^{ij}$ are obtained in different ways depending on the method used: FBS or GF.

For a fixed κ_n , the spectrum of the radial Dirac equation is non-degenerate, so it is convenient to introduce the index i_n that enumerates solutions for the given angular symmetry:

$$\begin{cases} \left(-\frac{d}{dr} + \frac{\kappa_n - 1}{r} \right) f_{i_n \kappa_n} + (V + m_e) g_{i_n \kappa_n} = \varepsilon_{i_n \kappa_n} g_{i_n \kappa_n}, \\ \left(\frac{d}{dr} + \frac{\kappa_n + 1}{r} \right) g_{i_n \kappa_n} + (V - m_e) f_{i_n \kappa_n} = \varepsilon_{i_n \kappa_n} f_{i_n \kappa_n}. \end{cases} \quad (25)$$

Then, Eq. (7) results for, e.g., G^{11} in

$$G_{\kappa_n}^{11}(\omega, r_1, r_2) = \sum_{i_n} \frac{g_{i_n \kappa_n}(r_1) g_{i_n \kappa_n}(r_2)}{\omega - \varepsilon_{i_n \kappa_n}^-}. \quad (26)$$

We stress that the index i_n in Eq. (26) and similar expressions runs over both the positive- and negative-energy Dirac continua as well as all bound states for the chosen κ_n . When using the DKB approach, for each κ_n the spectrum of the radial Dirac equation (25) is replaced with the finite set of solutions. In this case, the index i_n runs over these finite sets. When using the GF approach, the radial Green's function $G_{\kappa_n}^{ij}$ can be constructed from the solutions of the homogeneous Dirac equation, which are bounded at zero, $\phi_{\kappa_n}^0 = (g_{\kappa_n}^0 \ f_{\kappa_n}^0)^T$, and at infinity, $\phi_{\kappa_n}^\infty = (g_{\kappa_n}^\infty \ f_{\kappa_n}^\infty)^T$, (see, e.g., Ref. [48]):

$$G_{\kappa_n}(\omega, r_1, r_2) = \phi_{\kappa_n}^\infty(r_1) \phi_{\kappa_n}^{0T}(r_2) \theta(r_1 - r_2) + \phi_{\kappa_n}^0(r_1) \phi_{\kappa_n}^{\infty T}(r_2) \theta(r_2 - r_1). \quad (27)$$

Note that the solutions ϕ^0 and ϕ^∞ are supposed here to be normalized so that their Wronskian equals one. Expressions similar to Eqs. (24)-(27) can also be obtained for the free-electron Green's function, which we will denote as $G^{(0)}$.

With this in mind, we construct the many-potential part of the bound-electron Green's function which involves two or more interactions with the binding potential and corresponds to the last term in the expression (11):

$$G^{(2+)}(\omega, \mathbf{r}_1, \mathbf{r}_2) = \int d^3 \mathbf{x} \int d^3 \mathbf{y} G^{(0)}(\omega, \mathbf{r}_1, \mathbf{x}) V(x) G(\omega, \mathbf{x}, \mathbf{y}) V(y) G^{(0)}(\omega, \mathbf{y}, \mathbf{r}_2). \quad (28)$$

Since the potential V is assumed to be spherically symmetric, angular integrations in Eq. (28) can be easily carried out. As a result, one obtains the same PW expansion for $G^{(2+)}$ as that for G in Eq. (24). The radial components of $G^{(2+)}$ read as

$$G_{\kappa_n}^{(2+)ij}(\omega, r_1, r_2) = \sum_{\kappa, m} \int dx x^2 \int dy y^2 G_{\kappa_n}^{(0)ik}(\omega, r_1, x) V(x) G_{\kappa_n}^{km}(\omega, x, y) V(y) G_{\kappa_n}^{(0)mj}(\omega, y, r_2). \quad (29)$$

In the GF case, because of the θ -functions, radial integrations need to be handled carefully in Eq. (29), see, e.g., Ref. [78]. In the framework of the DKB approach, it is convenient to rewrite $G^{(2+)}$ in the form:

$$G^{(2+)}(\omega) = \sum_n \frac{|\tilde{n}\rangle \langle \tilde{n}|}{\omega - \varepsilon_n^-}, \quad (30)$$

where the new states $|\check{n}\rangle$ are defined by:

$$|\check{n}\rangle = \sum_f \frac{|f\rangle\langle f|V|n\rangle}{\omega - \varepsilon_f} \equiv \begin{pmatrix} \check{g}_{i_n\kappa_n}(r)\chi_{\kappa_n m_n}(\hat{\mathbf{r}}) \\ i\check{f}_{i_n\kappa_n}(r)\chi_{-\kappa_n m_n}(\hat{\mathbf{r}}) \end{pmatrix}. \quad (31)$$

Then, using Eq. (31), the many-potential contribution is expressed as:

$$\Delta\varepsilon_a^{\text{MP}} = \frac{i}{2\pi} \int_{-\infty}^{\infty} d\omega \sum_n \frac{\langle a\check{n}|I(\omega)|\check{n}a\rangle}{\varepsilon_a - \omega - \varepsilon_n^-}. \quad (32)$$

The expression (32) can be readily adjusted to be used within the GF approach. For this aim, one needs to reverse an expression similar to Eq. (26):

$$\sum_{i_n} \frac{\check{g}_{i_n\kappa_n}(r_1)\check{g}_{i_n\kappa_n}(r_2)}{\omega - \varepsilon_n^-} \rightarrow G_{\kappa_n}^{(2+)}(\omega, r_1, r_2). \quad (33)$$

The matrix element of the operator $I(\omega)$ can be expressed as follows:

$$\langle ab|I(\omega)|cd\rangle = \sum_{JM} (-1)^{j_a - m_a + J - M + j_b - m_b} \begin{pmatrix} j_a & J & j_c \\ -m_a & M & m_c \end{pmatrix} \begin{pmatrix} j_b & J & j_d \\ -m_b & -M & m_d \end{pmatrix} \langle ab||I(\omega)||cd\rangle_J, \quad (34)$$

where the reduced matrix elements, $\langle ab||I(\omega)||cd\rangle_J$, on the right-hand side do not depend on the angular-momentum projections. Their explicit forms in the Feynman and Coulomb gauges are given in Appendix C in Eqs. (C2) and (C3), respectively. Finally, the summation over the projections m_n in Eq. (32) can be done analytically, and we obtain:

$$\Delta\varepsilon_a^{\text{MP}} = \frac{i}{2\pi} \sum_{\kappa_n} \int_{-\infty}^{\infty} d\omega \sum_{J, i_n} \frac{(-1)^{j_n - j_a + J}}{2j_a + 1} \frac{\langle a\check{n}|I(\omega)|\check{n}a\rangle_J}{\varepsilon_a - \omega - \varepsilon_n^-}. \quad (35)$$

The sums over J and κ_n in Eq. (35) are not independent due to the triangular inequality. In our calculations, the sum over κ_n is considered as the primary one. As a result, the many-potential contribution is represented by the sum of the often poorly converging PW-expansion series in κ_n . To calculate it, one has to resort to the procedure of extrapolation in $k = |\kappa_n|$. In what follows, we for brevity will use κ instead of κ_n , if this does not lead to misunderstandings.

D. Partial-wave expansion acceleration schemes

The convergence of the PW-expansion series could be improved using different acceleration schemes. Their general idea is to separate out and subtract the term $\Delta\varepsilon_{a,x}^{\text{subtr}}$, which contains the slowly converging part of the PW expansion of the many-potential contribution. The index “ x ” in $\Delta\varepsilon_{a,x}^{\text{subtr}}$ indicates that the subtracted term should be calculated exactly in the same manner as $\Delta\varepsilon_a^{\text{MP}}$, that is in coordinate space using the PW expansion. Naturally that the same term, evaluated separately, but not necessarily within the same approach, so we denote it as $\Delta\varepsilon_a^{\text{subtr}}$ without the additional index “ x ”, should then be added back. The discussed idea can be illustrated by the formula:

$$\Delta\varepsilon_a^{\text{MP}} \rightarrow (\Delta\varepsilon_a^{\text{MP}} - \Delta\varepsilon_{a,x}^{\text{subtr}}) + \Delta\varepsilon_a^{\text{subtr}}. \quad (36)$$

It is implied that the PW-expansion series for the two contributions in the brackets in Eq. (36) are subtracted term by term and only then extrapolated in k . The resulting difference is expected to demonstrate a better convergence (at least, in terms of absolute values) than the initial series for the many-potential contribution. Therefore, if one can calculate $\Delta\varepsilon_a^{\text{subtr}}$ with high accuracy, it will determine the overall improvement in the calculations of the many-potential contribution to the SE correction.

Within the two-potential acceleration scheme (see the Introduction section), the subtracted term is the two-potential contribution, $\Delta\varepsilon_{a,x}^{\text{subtr}} = \Delta\varepsilon_{a,x}^{2p}$. When adding this term back, one must evaluate it with high precision in order to benefit from applying the scheme. A natural idea is to perform the corresponding calculations in momentum space without using the PW expansions. However, this problem is complicated and leads to complex multidimensional integrals, see, e.g., Ref. [72], where a similar approach was employed in the point-nucleus case for the SE correction to the hyperfine splitting. For this reason, an alternative was proposed in Refs. [78, 79], where the difference between the many- and two-potential terms was addressed using the FBS method, while the two-potential term itself was also considered in coordinate space but employing the GF method and truncating the corresponding PW summations at higher values

of angular momenta. We note that in this case, it is not necessary to solve the system of differential equations numerically for an arbitrary potential, since the PW expansion of the free-electron propagator can be expressed in terms of the spherical Bessel functions [2] and the desired two-potential term can be obtained by combining three such propagators. In the present work, we study this two-potential scheme but for simplicity the difference between the many- and two-potential terms is also treated based on the GF approach. The PW expansion for this difference arises from the Green's function

$$G^{(3+)} = G^{(2+)} - \sum_{f_1, f_2, f_3} \frac{|f_1\rangle\langle f_1|V|f_2\rangle\langle f_2|V|f_3\rangle\langle f_3|}{(\omega - \varepsilon_{f_1}^-)(\omega - \varepsilon_{f_2}^-)(\omega - \varepsilon_{f_3}^-)}. \quad (37)$$

We refer to the term corresponding to $G^{(3+)}$ as the three-plus-potential contribution, $\Delta\varepsilon_a^{(3+)p} \equiv (\Delta\varepsilon_a^{\text{Mp}} - \Delta\varepsilon_{a,x}^{2p})$.

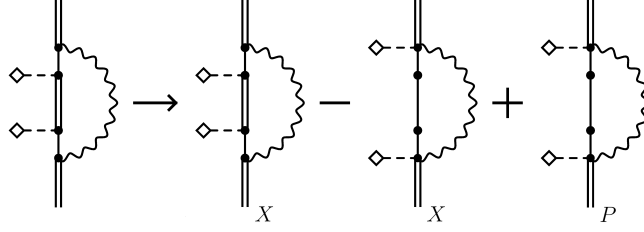


Figure 3. Diagrammatic representation of the quasi-two-potential term separation. The last term on the right side is calculated in momentum space without using any PW expansion.

The Sapirstein-Cheng (SC) scheme [73] is based on the idea that the dominant contribution from the free-electron propagators $G^{(0)}(\omega, \mathbf{r}_1, \mathbf{r}_2)$ comes from the region where both their spatial arguments are close to each other [45], $\mathbf{r}_1 \approx \mathbf{r}_2$. Therefore, one can obtain an approximation to the two-potential term by “transposing” the potentials from the inner electron line to the vertices, where the photon propagator is attached, see Fig. 3. We refer to this approximation as the quasi-two-potential term and denote it as $\Delta\varepsilon_{a,x}^{\text{subtr}} = \Delta\varepsilon_{a,x}^{2p}$. The difference between the many- and quasi-two-potential terms, $\Delta\varepsilon_{a,x}^{(3+)p} \equiv \Delta\varepsilon_a^{\text{Mp}} - \Delta\varepsilon_{a,x}^{2p}$, referred to as the quasi-three-plus-potential contribution, can be studied in the coordinate space using the PW expansion for the Green's function

$$\tilde{G}^{(3+)} = G^{(2+)} - \sum_f \frac{|Vf\rangle\langle fV|}{(\varepsilon_a - \omega - \varepsilon_f^-)^3} \quad (38)$$

Here, $|Vf\rangle = V|f\rangle$. A solid advantage of the SC scheme is the fact that it is fairly easy to calculate the quasi-two-potential contribution with high accuracy in momentum space. We denote the result as $\Delta\varepsilon_{a,p}^{2p}$ and use it as $\Delta\varepsilon_a^{\text{subtr}}$. The potentials that have been transposed into vertices can be formally taken into account by multiplying the wave function of the external state $|a\rangle$ by them. An issue arises of calculating the Fourier transform of such products. Since V is assumed to be spherically symmetric, this can be done by a straightforward generalization of Eqs. (13)-(15). We represent the result in the following form:

$$\phi_a(\mathbf{p}) = \int d^3\mathbf{r} e^{-i(\mathbf{p}\cdot\mathbf{r})} V(r) \psi_a(\mathbf{r}) = i^{-l_a} \left(\begin{array}{c} \tilde{t}_a(p) \chi_{\kappa_a m_a}(\hat{\mathbf{p}}) \\ \tilde{s}_a(p) \chi_{-\kappa_a m_a}(\hat{\mathbf{p}}) \end{array} \right), \quad (39)$$

$$\tilde{t}_a(p) = 4\pi \int_0^\infty dr r^2 j_{l_a}(pr) V(r) g_a(r), \quad (40)$$

$$\tilde{s}_a(p) = -4\pi \frac{\kappa_a}{|\kappa_a|} \int_0^\infty dr r^2 j_{2j_a - l_a}(pr) V(r) f_a(r). \quad (41)$$

Using the identity

$$\int d\mathbf{y} d\mathbf{z} G^{(0)}(\omega, \mathbf{x}_1, \mathbf{y}) G^{(0)}(\omega, \mathbf{y}, \mathbf{z}) G^{(0)}(\omega, \mathbf{z}, \mathbf{x}_2) = \frac{1}{2} \frac{\partial^2}{\partial \omega^2} G^{(0)}(\omega, \mathbf{x}_1, \mathbf{x}_2), \quad (42)$$

one obtains

$$\Delta\varepsilon_{a,p}^{2p} = \frac{1}{2} \int \frac{d^3\mathbf{p}}{(2\pi)^3} \bar{\phi}_a(\mathbf{p}) \left. \frac{\partial^2 \Sigma_R^{(0)}(\mathbf{p})}{\partial p_0^2} \right|_{p_0=\varepsilon_a} \phi_a(\mathbf{p}), \quad (43)$$

where $\mathbf{p} = (p_0, \mathbf{p})$. The explicit form of the derivatives of the free-electron self-energy operator $\Sigma_R^{(0)}$ with respect to p_0 in both gauges is given in Appendix D. After performing the angular integration, which is carried out similarly to that in the zero-potential contribution, one can obtain:

$$\Delta\tilde{\varepsilon}_{a,p}^{2\text{p}} = \frac{\alpha}{8\pi} \int \frac{dpp^2}{(2\pi)^3} [N_1 (\tilde{t}_a^2 - \tilde{s}_a^2) + N_2 (\tilde{t}_a^2 + \tilde{s}_a^2) + 2pN_3\tilde{t}_a\tilde{s}_a] \quad (44)$$

where N_1 , N_2 , and N_3 are defined in Appendix D, $\tilde{t}_a = \tilde{t}_a(p)$ and $\tilde{s}_a = \tilde{s}_a(p)$.

III. COMPUTATIONAL DETAILS

The calculations are carried out by means of two approaches: the FBS method within the DKB basis and the GF method. The methods differ only in the treatment of the terms evaluated in coordinate space. The momentum-space contributions are the same in both approaches.

A. Momentum-space calculations

The contributions evaluated in momentum space include the zero- and one-potential terms resulting from the renormalization procedure, as well as the quasi-two-potential terms corresponding to the SC convergence-acceleration scheme. All the integrals in the zero-, one-, and quasi-two-potential terms are calculated using the Gauss-Legendre quadratures. Let us first briefly discuss an evaluation of the zero-potential terms. The domain of integration over p is divided into two parts, $p \leq p_0$ and $p \geq p_0$, where $p_0 = \alpha Z$. The integration over the second domain can be carried out using a change of variables of the form $t = \alpha Z/p$, as a result of which the ray $[\alpha Z, \infty)$, is mapped onto the interval $[1, 0]$. The first domain is finite, so its treatment causes no problems. Compared to the Feynman gauge, the zero-potential contribution in the Coulomb gauge contains an additional integration over the Feynman parameter x , see Eqs. (17), (A10), and (A11). The coefficient F_2 in Eq. (A11) must be calculated as a principal-value integral. From a numerical point of view, it is helpful to isolate the singularity. We do that by adding and subtracting the same integrand but with the numerator evaluated at the singularity point $x = a$:

$$\int dx \frac{F(x)}{x - a + i0} = \int dx \frac{F(x) - F(a)}{x - a + i0} + \int dx \frac{F(a)}{x - a + i0}. \quad (45)$$

The first term in the right-hand side of Eq. (45) becomes regular. To avoid numerical problems at $x = a$, the exact expression can be replaced with its Taylor series in a small vicinity of this point. The second term in Eq. (45) is calculated analytically. Similar methods can be used to calculate $\Delta\tilde{\varepsilon}_a^{2\text{p}}$ in momentum space. To avoid possible numerical problems due to large cancellations, one should use the Taylor-series expansion for the corresponding integrands.

The evaluation of the one-potential contributions involves the integrations over the variables p , p' , z , and a number of Feynman parameters. When integrating over the Feynman parameters in both gauges, to avoid possible numerical errors, the Taylor series for the integrands are employed. In the Coulomb-gauge case we use the results of Ref. [80], but expand all the coefficients $F_1 - F_{21}$ at “suspicious” points. The expression (20) has an integrable singularity for $q = 0$ when $p = p'$ and $z = 1$. Therefore it is necessary to properly choose integration nodes for the variable z to ensure the integral convergence. For this goal, we use the transformation $z = 1 - 2t^2$ with $t \in [0, 1]$. To calculate the integrals over the variables p and p' , we change the variables according to $P = (p + p')/\sqrt{2}$ and $P' = (p - p')/\sqrt{2}$. The integral over P is calculated similar to the integral over p for the zero-potential contribution, but the separation point $p_0 = 2\alpha Z$ is chosen instead. The integral over P' is taken within the finite interval $[-P, P]$.

To estimate an uncertainty of the momentum-space calculations, the number of quadrature nodes and position of the separation points p_0 are varied.

B. Coordinate-space calculations

The calculation of all coordinate-space contributions, many-potential, two-potential, and (quasi-) three-plus-potential terms, has many common points. Let us illustrate them with an example of the many-potential contribution. Its evaluation essentially reduces to the calculation of three integrals: over the radial variables r_1 and r_2 , see Eqs. (C2) and (C3), and over the energy parameter ω . Taking into account the exponential decay of bound-electron

wave functions at large distances, all radial integrations are performed over the finite interval $[0, R_{\max}]$. The value of the parameter R_{\max} is chosen so that the results are independent of it within the desired accuracy. All the radial integrations are carried out using the Gauss–Legendre quadratures. However, the specific details differ slightly in the DKB and GF approaches.

In the DKB approach, the domain $[0, R_{\max}]$ is divided into a finite number of intervals by the nodes used to construct the B splines. The integration method for the double integral over r_1 and r_2 depends on whether these variables belong to the same interval or not. If not, the integrations are carried out independently using the same quadrature for both variables. However, when r_1 and r_2 fall into the same interval, a more delicate integration is employed to take into account the fact that the integrand depends on $r_< = \min\{r_1, r_2\}$ and $r_> = \max\{r_1, r_2\}$. Namely, for some fixed value of r_1 the corresponding interval is divided into two subintervals lying to the left and to the right from r_1 . The integration over r_2 is performed by using the Gauss–Legendre quadratures for both subintervals. Note that within the DKB approach, the integration over radial variables turns out to be “tied” to the size of the basis N . As the FBS size grows, the number of nodes also increases, that leads to the improvement of the integration accuracy. Thus, the single parameter N affects both the accuracy of the Green’s function representation and the integration accuracy.

In the GF approach, the radial integrations become more complicated due to the aforementioned discontinuities of the electron Green’s functions. The integrations over x and y in Eq. (28) cannot be performed independently of the integrations over r_1 and r_2 . To evaluate the radial integrals, we employ a variation of the method described, e.g., in Ref. [48]. Namely, a hierarchy of the radial integration grids is prepared, with each subsequent grid becoming finer and “lying” inside the previous one. Then, all the radial integrations are arranged in the following order: r_1 , r_2 , x , and y . Therefore, the finest grid corresponds to the variable y . The accuracy of the GF approach is determined mainly by the accuracy of the radial integrations.

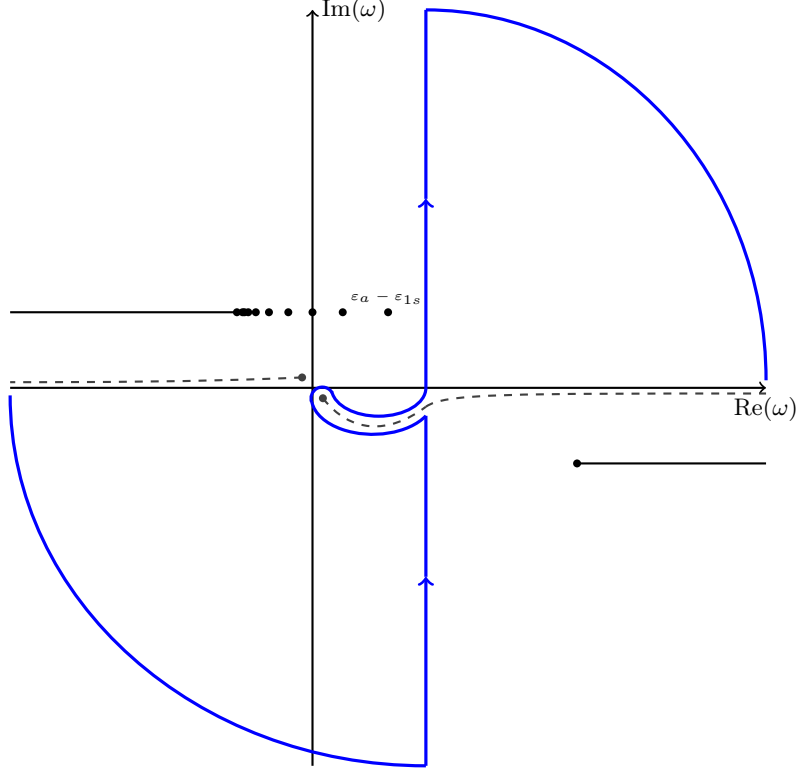


Figure 4. Deformed contour (blue solid line) in the complex plane ω . Singularities and branching cuts of the electron Green’s function (black lines and black dots) and photon propagator (black dashed lines) are shown.

The photon and electron propagators have a complicated analytical structure as functions of the energy parameter ω in the complex plane. They are two-valued functions and are defined on the corresponding Riemann surfaces with two sheets (for each propagator). Fig. 4 shows the complex plane of the integration variable ω , the branch points of both propagators with the cuts starting from them, and the poles of the electron propagator corresponding to the bound states. In the expression for the SE correction (3), the integration contour goes along the real axis, but it can be bended in the ω complex plane to “simplify” the calculations. Because of the zero photon mass, the contour is squeezed between two infinitely close branching points near zero. Introducing a finite mass would allow them to

be pushed apart, which can be easily demonstrated in the Feynman gauge. Consequently, the contour must always pass through $\omega = 0$. In principle, there is no other restrictions on the contour. Thus, it can be changed as needed, respecting the analytical structure of the integrand.

In this work, the approach proposed in Ref. [65] is used. Namely, we employ the transformation that results in the contour shown in Fig. 4. The original contour along the real axis is rotated and deformed. The contributions from the circular arcs vanish as the radius of the circle tends to infinity, so we do not consider them. The rotation is done to avoid fast oscillations of the integrand encountered on the real axis: on the vertical parts of the deformed contour the integrand decays exponentially. The deformation of the contour near zero and its shift to the right from the imaginary axis is done to avoid going close to the poles of the electron Green's function, which correspond to the bound states with binding energies no less than that of the state under consideration. For large enough values of κ , the contour simplifies and can be taken along the imaginary axis. The integration over ω is evaluated using the Simpson quadratures. The number of integration points is increased until the required accuracy is achieved.

C. Extrapolation of the PW-expansion sums

We obtain a coordinate-space contribution as a PW series in κ , which should inevitably be truncated at some $|\kappa_{\max}|$. The remainder of the series can then be estimated using an extrapolation procedure. The extrapolation methods discussed below are applied to all treated coordinate-space contributions. Here and in what follows, when discussing partial sums, we will denote by the index $k > 0$ the sum of all terms of the PW expansion with $|\kappa| \leq k$.

When using the DKB method, the individual contributions strongly depend on the FBS size N , therefore, an extrapolation over this parameter is also required. In this case, the most stable results are obtained if one extrapolates with respect to the basis size first. Let us denote as $S_k(N)$ the partial sum obtained for the given FBS size N . For each k , the extrapolation over N is performed using a non-linear least-squares method using an ansatz of the form:

$$S_k(N) = A_k \left(\frac{1}{N} \right)^{B_k} + S_k, \quad (46)$$

where S_k are the extrapolated to the infinite basis set partial sums, and A_k and B_k are adjustable numerical coefficients. In the GF approach, the sums S_k are obtained directly from the calculations, and this extrapolation is not required.

To extrapolate over k in both DKB and GF approaches, we implement three following ansatzes for the partial sums S_k :

$$\tilde{S}(k) = S_\infty + \frac{C_2}{k^2} + \frac{C_3}{k^3} + \dots + \frac{C_m}{k^m}, \quad (47)$$

where the parameter S_∞ and coefficients C_i for $i = 2, \dots, m$ (with m being 4, 5 and 6) are obtained by a kind of statistical method. Namely, for each m , N_{iter} times a subset of k 's, $\{k_i\}_{i=1}^m$, is randomly selected. The parameter N_{iter} is fixed by the condition that all possible subsets are considered for the largest m ($m = 6$). For each element of the above subsets we construct and solve the system of m linear equations of the form

$$\tilde{S}(k_i) = S_{k_i}, \quad i = 1, \dots, m \quad (48)$$

to determine m variables $S_\infty, C_2, \dots, C_m$. Repeating this step $3N_{\text{iter}}$ times yields a set of approximations for S_∞ . Evaluating the mean value \bar{S}_∞ and variance σ_k , one obtains the desired extrapolated sum and an estimation for its uncertainty. We note that we approximate the tails only (by excluding the first few k 's from consideration). Changing the tail size produces results that are consistent with each other.

Within the DKB approach, the uncertainties of extrapolation in k , σ_k , and extrapolation to an infinite basis set, σ_N , are summed quadratically

$$\sigma_{\text{tot}} = \sqrt{\sigma_\kappa^2 + \sigma_N^2}. \quad (49)$$

Example of the use of this two-step extrapolation procedure can be found in the ‘‘results’’ section below.

IV. RESULTS

In the present work, we conduct two sets of SE-correction calculations. First, we consider the $1S_{1/2}$ state in three hydrogen-like ions: argon ($Z = 18$), xenon ($Z = 54$), and uranium ($Z = 92$). We adopt the results from Ref. [69] as a benchmark for comparison. For this reason, in the first part of calculations, the values of root-mean-square (rms) nuclear radii as well as the values of fundamental constants, e.g., the fine-structure constant α and the Hartree energy in eV, are taken to be the same as there. The obtained data are used to analyze the convergence of the many-potential contribution. Second, we study the SE corrections for the $1S_{1/2}$, $2S_{1/2}$, $2P_{1/2}$, and $2P_{3/2}$ states in a set of hydrogen-like ions with the nuclear charge Z in the range from $Z = 10$ to $Z = 100$ and compare the obtained results with the ones presented in Ref. [26]. In this case, the rms radii and models of the nuclear-charge distribution are chosen to coincide with those in the corresponding work, however, for α the numerical value from the CODATA (2018) [81] is used. In the second part, the SE correction is represented in terms of the dimensionless function $F(\alpha Z)$, defined as:

$$\Delta\varepsilon_a = \frac{\alpha}{\pi} \frac{(\alpha Z)^4}{n^3} F(\alpha Z) mc^2. \quad (50)$$

The data obtained in the second part of the work are used to analyze the acceleration-convergence schemes.

A. Many-potential term: convergence analysis

Let us start with illustrating the two-step extrapolation procedure, described in the previous section, using the ground state of hydrogen-like xenon ($Z = 54$) as an example, see Fig. 5. The many-potential term is considered, and the results for both gauges are presented. At the first stage, the extrapolation of the partial sums $S_k(N)$ with respect to the size of the basis N is performed. For convenience, only the extrapolation curves for $k = 10, 15,$ and 20 are shown as functions of $1/N$. The corresponding extrapolated sums $S_{10}, S_{15},$ and S_{20} are depicted as stars at $1/N \rightarrow 0$. The extrapolated partial sums S_k obtained for other values of k are depicted with dashes as well. At the second stage, the extrapolation over k is performed. The final values for $\Delta\varepsilon_a^{\text{MP}} = S_\infty$ are shown with black squares. Note that the GF method yields results that are indistinguishable at this scale from those obtained by the DKB method. Based on our experience, a small difference in the FBS size extrapolation in the two gauges appears in the small- Z region, where the convergence behavior is slightly better in the Coulomb gauge. In the region of medium- and large- Z there is no significant difference between the gauges. This can be seen, e.g., from Fig. 5, where the absolute values of the many-potential terms in two gauges differ by approximately one order of magnitude, while the rate of convergence in the FBS size is approximately the same.

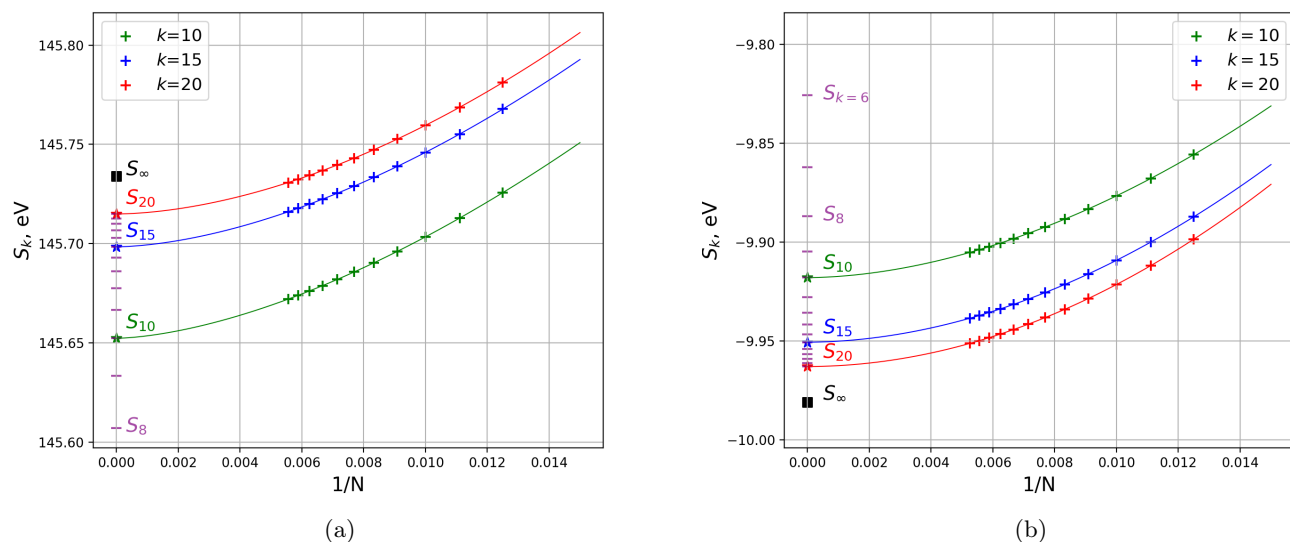


Figure 5. The extrapolation of the many-potential contribution to the self-energy correction for the $1S_{1/2}$ state of hydrogen-like xenon ($Z = 54$) obtained within the framework of the DKB approach in the Feynman (a) and Coulomb (b) gauges.

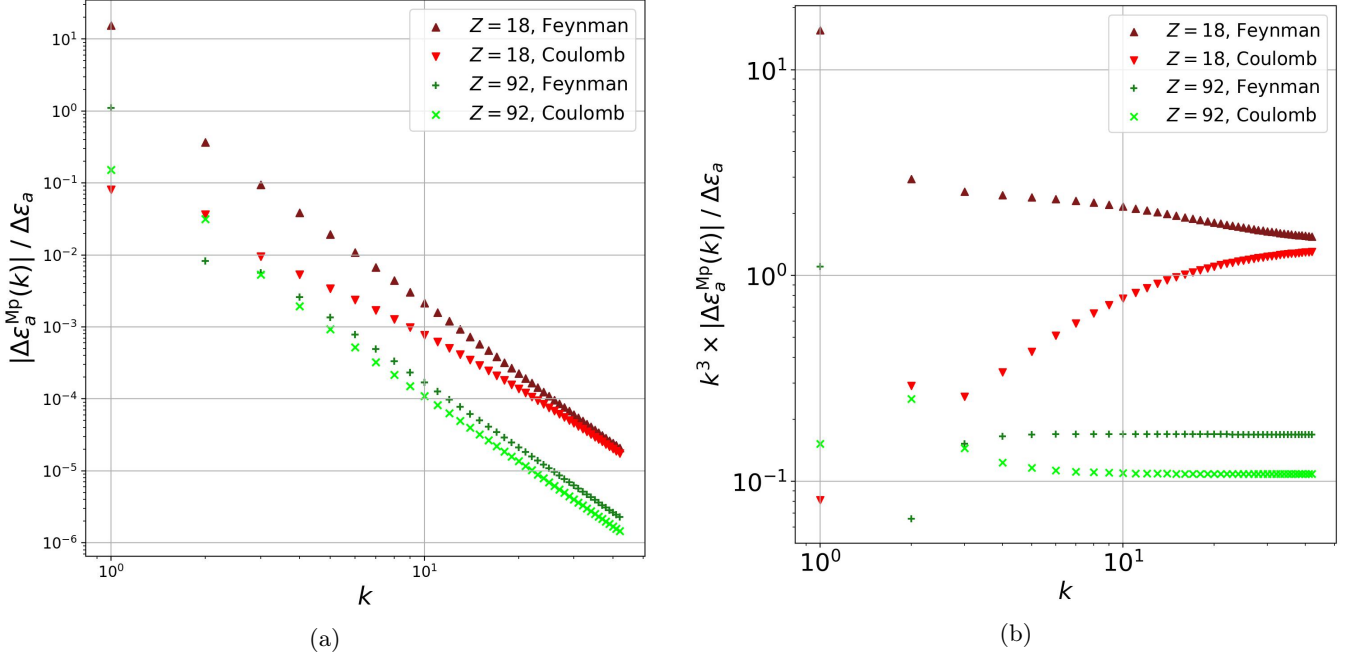


Figure 6. The individual many-potential contributions $\Delta\varepsilon_a^{\text{MP}}(k)$: (a) normalized to the total self-energy correction $\Delta\varepsilon_a$ and (b) additionally multiplied by k^3 . Note the log-log scale.

Let us now examine in details the PW convergence of the many-potential contributions and perform a comparative analysis within two gauges. The zero-, one-, and many-potential contributions to the SE correction for the $1S_{1/2}$ state in hydrogen-like argon ($Z = 18$) and uranium ($Z = 92$) in Feynman and Coulomb gauges are presented in Table I. For the many-potential contributions, the individual terms of the PW expansion, $\Delta\varepsilon_a^{\text{MP}}(k)$, obtained by means of the GF approach are shown. These terms represent sums of contributions with $\kappa = k$ and $\kappa = -k$, i.e., the partial sums are given by $S_k = \sum_{i=1}^k \Delta\varepsilon_a^{\text{MP}}(i)$. The row labeled “ $\sum_{k=1}^{24}$ ” gives the partial sums S_{24} , while the subsequent row “ $\sum_{k=25}^{\infty}$ [extr.]” provides our estimations for the remainders of PW series obtained by applying the statistical extrapolation procedure discussed above. The total SE corrections are presented in the last line.

For convenience, the absolute values of the individual terms $\Delta\varepsilon_a^{\text{MP}}(k)$ from Table I, normalized to the total self-energy correction $\Delta\varepsilon_a$, are plotted in Fig. 6(a). From Table I and Fig. 6(a), it can be noticed that for both considered Z the many-potential contributions as well as the first terms of the PW expansions are significantly smaller in the Coulomb gauge (in the case of $Z = 18$, by two orders of magnitude) than in the Feynman gauge. This difference, however, becomes much less noticeable for large values of k , although the Feynman-gauge contributions still exceed their Coulomb-gauge counterparts.

Multiplying the individual terms $\Delta\varepsilon_a^{\text{MP}}(k)$ obtained for two gauges by the factor of k^3 provides a more informative comparison of their decay rate with the growth of k , that is demonstrated in Fig. 6(b). Let us discuss the leading asymptotic behavior of the PW-expansion terms for $k \rightarrow \infty$: $\Delta\varepsilon_a^{\text{MP}}(k) \sim 1/k^p$. Our numerical results indicate that in both the Feynman and Coulomb gauges, the exponent p exceeds 2 over a wide range of Z , with p being close to 3 in the large- Z region. These conclusions do not contradict those from Ref. [74], where it was claimed that in the Feynman gauge $p = 3$ regardless of the nuclear charge Z . The latter observation justifies the fact that the ansatz for the extrapolation over k in (47) starts from $1/k^2$, since $\sum_{i=1}^k 1/i^3 \sim 1/k^2$.

We also note that the numerical coefficients for the higher powers of $1/k$ in the expansion (47) in the Coulomb gauge are larger than their Feynman-gauge counterparts. That fact is also illustrated in the Fig. 6(b) – convergence to asymptotics in the Feynman gauge is significantly slower. As a result, within the k -range studied in the present work ($k \leq 20$ or $k \leq 24$), the leading asymptotic behavior is less pronounced in the Coulomb gauge. The latter fact apparently balances out the smallness of the absolute value of the Coulomb-gauge many-potential contribution. In practice, within the GF approach, given the same resource costs (number of partial waves, number of integration nodes for radial variables, etc.), the Coulomb and Feynman gauges are equally suitable for estimating the many-potential contribution to the SE correction within a wide range of nuclear charges Z . This conclusion slightly contradicts what was claimed in Ref. [70]. Nevertheless, we agree with the fact that the advantages of the Coulomb gauge are the improved convergence of the many-potential contributions over the basis-set size in the small- Z region, relative smallness of the many-potential contribution [69, 70], and the absence of cancellation between different parts of the

SE correction.

B. Application of the convergence-acceleration schemes

Now let us turn to the comparative analysis of the SC and two-potential schemes used to accelerate the convergence of the PW expansions for the many-potential contributions in the Feynman and Coulomb gauges. In Fig. 7(a), ratios of the three-plus-potential $\Delta\varepsilon_{a,x}^{(3+)P}$ and quasi-three-plus-potential $\Delta\tilde{\varepsilon}_{a,x}^{(3+)P}$ contributions to the total many-potential contributions $\Delta\varepsilon_a^{\text{MP}}$ are plotted. In the low- Z region, the two-potential scheme in Coulomb gauge yields the smallest remainder which is to be extrapolated. However, in this case the overall accuracy is limited by the two-potential contribution, which also has to be treated within the PW expansion.

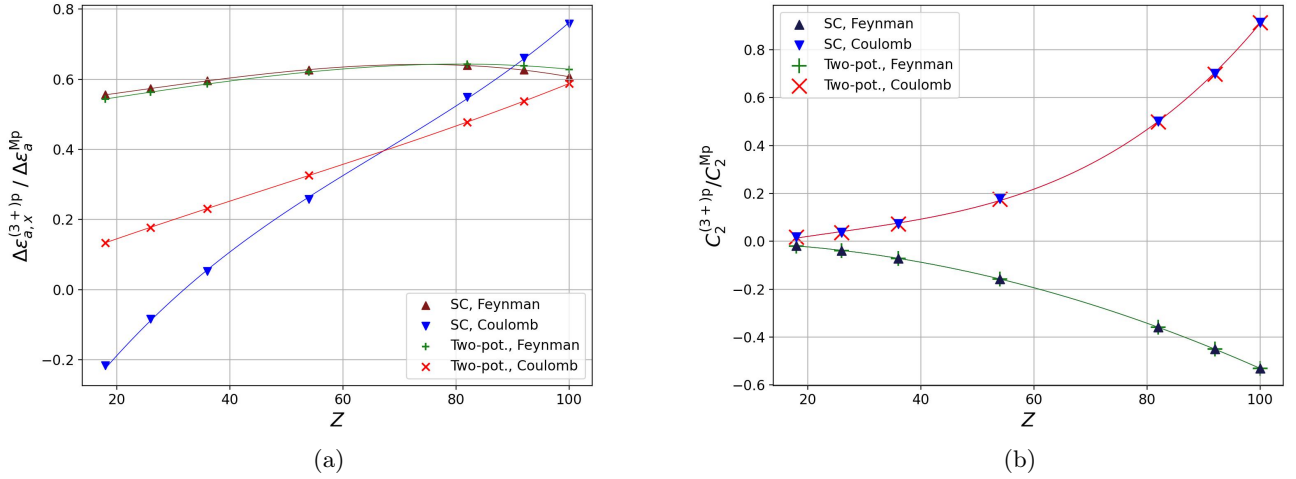


Figure 7. Comparison of two convergence-acceleration schemes in two gauges, Feynman and Coulomb ones: (a) three-plus-potential $\Delta\varepsilon_{a,x}^{(3+)P}$ and quasi-three-plus-potential $\Delta\tilde{\varepsilon}_{a,x}^{(3+)P}$ contributions normalized to the total many-potential contributions $\Delta\varepsilon_a^{\text{MP}}$; (b) the same for the coefficients C_2 defined in Eq. (47).

Let us turn to the coefficients C_2 from Eq. (47) obtained for $\Delta\varepsilon_{a,x}^{(3+)P}$ and $\Delta\tilde{\varepsilon}_{a,x}^{(3+)P}$ (designated as $C_2^{(3+)P}$) by means of our statistical extrapolation approach. These coefficients normalized to the coefficients C_2^{MP} for the corresponding many-potential contributions are shown in Fig. 7(b). These data partially explain the convergence-acceleration mechanism. In the area of low Z , the coefficients C_2 for the (quasi-)three-plus-potential contributions decrease by one or two orders of magnitude compared to their counterparts for the many-potential contributions. In the region of high Z , they also decrease, but less effectively. It should be noted that for each gauge the reduction of the coefficient C_2 for both studied acceleration schemes is almost identical, which confirms that the SC trick indeed provide a good approximation to the two-potential contribution.

The subtraction of the two-potential or quasi-two-potential contributions from the many-potential contribution apparently does not change the leading asymptotic behavior of the PW-expansion terms for the remainders $\Delta\varepsilon_a^{(3+)P}$ and $\Delta\tilde{\varepsilon}_a^{(3+)P}$ and only decreases the absolute values of the corresponding coefficients. To illustrate this, in Fig. 8 we plot the individual terms of the PW expansions for these remainders normalized to the total SE correction and additionally multiplied by k^3 , exactly as it was done in Fig. 6 for the many-potential contributions. One can see that the individual terms tend to constants in all the cases, i.e. $p = 3$ for (quasi-)three-plus potential terms. That statement has also been verified empirically: the extrapolation procedure gives obviously incorrect results if one omits the term C_2/k^2 in the Eq. (47). We stress that our conclusion contradicts the one from work [73]. Fig. 8 also demonstrates that for both acceleration schemes the approach to the asymptotics in the Coulomb gauge is much faster than in the Feynman gauge. The last statement makes it easier to extrapolate the corresponding contributions and certainly makes the Coulomb gauge more preferable for SE calculations within the convergence-acceleration schemes for a wide range of Z .

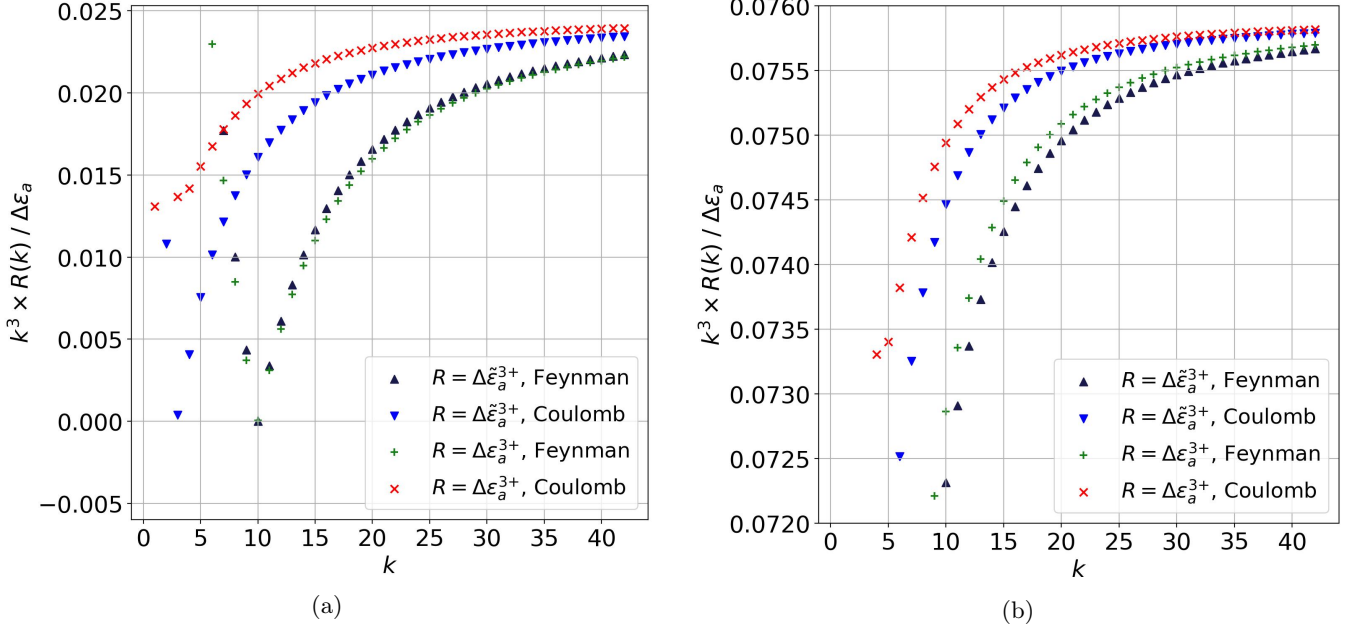


Figure 8. The individual contributions $\Delta\epsilon_a^{(3+)p}(k)$ and $\Delta\tilde{\epsilon}_a^{(3+)p}(k)$ normalized to the total SE correction and multiplied by the factor of k^3 : (a) for $Z = 18$ argon; (b) for $Z = 92$ uranium.

C. Data: summary

In this section, we present and discuss the results of our calculations of SE corrections to the $n = 1$ and $n = 2$ energy levels in hydrogen-like ions.

First, in Table II we study the SE correction for the ground $1S_{1/2}$ state of hydrogen-like argon ($Z = 18$), xenon ($Z = 54$), and uranium ($Z = 92$). As was noted above, Ref. [69] is considered to be the benchmark in this case. Therefore, in this part of the calculations, we adopt the values of the fundamental constants and nuclear parameters to be the same as those used in that work. For each ion, we consider two gauges, the Coulomb gauge and the Feynman gauge, which are indicated in the second column as “C” and “F”, respectively. The corresponding zero- and one-potential contributions, calculated in momentum space, are shown in the third and fourth columns. For each gauge we compare different numerical approaches to the evaluation of the many-potential contribution $\Delta\epsilon_a^{\text{MP}}$: (i) the standard method, labeled in the column “Scheme” as “DIR”, in which the many-potential contribution is treated as a whole; (ii) the two-potential acceleration scheme, labeled as “TP”, where this contribution is represented as the sum $\Delta\epsilon_a^{2p} + \Delta\epsilon_a^{(3+)p}$, and (iii) the Sapirstein-Cheng acceleration scheme, labeled as “SC”, where it is given by the sum $\Delta\tilde{\epsilon}_a^{2p} + \Delta\tilde{\epsilon}_a^{(3+)p}$. We also compare two methods for representing the electron propagators: the finite-basis-set method within the DKB basis and the Green’s function approach, which are indicated as “DKB” and “GF”, respectively. All the coordinate-space contributions, $\Delta\epsilon_a^{\text{MP}}$, $\Delta\epsilon_a^{2p}$, $\Delta\epsilon_a^{(3+)p}$, and $\Delta\tilde{\epsilon}_a^{(3+)p}$, are obtained by applying the statistical extrapolation procedure described in Sec. III C. Within the DKB approach, the PW-expansion series are truncated at $|\kappa_{\text{max}}| = 20$. When using the GF approach, these series are truncated at $|\kappa_{\text{max}}| \sim 45$ in the case of the two-potential contribution $\Delta\epsilon_a^{2p}$ and at $|\kappa_{\text{max}}| = 24$ in the other cases. Finally, the total SE corrections obtained by means of different approaches are given in the last column. For each ion and gauge, the results from Ref. [69] are shown for comparison as well.

As can be seen from Table II, the main source of numerical errors, regardless of the gauge, is the many-potential contribution. Even when applying the acceleration schemes, this contribution still limits the accuracy of the total SE corrections. We note that the many-potential contribution is significantly smaller in the Coulomb gauge than in the Feynman gauge (see the penultimate column in Table II), which was also noticed in Refs. [69, 70]. However, for the reasons described above, this does not provide a significant increase in accuracy unless acceleration schemes are involved. Although obtaining the zero- and one-potential contributions with sufficient accuracy is not a technically difficult task, an attractive feature of the Coulomb gauge, as can be seen from Table II, is the absence of large cancellations between these momentum-space contributions. Nevertheless, this observation is extremely useful for obtaining high-precision results for low- Z systems.

Clearly, acceleration tricks reduce extrapolation uncertainties and allow for a more accurate evaluation of the many-

potential contributions. Using either the two-potential scheme or the SC scheme reduces the numerical errors and allows one to obtain up to two additional significant digits. As a rule, the most accurate many-potential contribution can be obtained by using a combination of the Coulomb gauge and the SC acceleration scheme.

The GF approach provides a more accurate treatment of the many-potential contribution compared to the DKB approach. This results mainly not from the lower value of $|\kappa_{\max}|$ employed in this case, but from the fact that the DKB method needs the approximation with respect to the size of the basis set. The low accuracy of the DKB approach does not detract from the already mentioned advantages, namely, the ability to exclude a specific state and construct Green's functions for a wider class of systems that do not possess spherical symmetry. In some sense, the FBS method (not necessarily in the DKB realization) is more flexible and easier to implement. Therefore, if high accuracy is not required, it is an excellent method for calculating the SE correction.

Returning to the comparison with the benchmark calculations [69], we note that our results obtained by means of different methods are in good agreement with each other and those from Ref. [69]. Small deviations have been revealed. However, the reason for them is unclear for us.

For a broader comparison, another set of calculations has been performed. Namely, we consider the SE correction for the ground $1S_{1/2}$ state in hydrogen-like ions with $Z \in \{10, 18, 26, 36, 54, 82, 92, 100\}$. In this case, we compare our results with those from Ref. [26]. Therefore, the nuclear parameters are taken from Ref. [26]. Average values of rms nuclear radii from there were used. An estimation of the uncertainty of the SE correction with respect to the nuclear radius and nuclear model is beyond the scope of the current paper, the interested reader can find it in the original work [26]. The values of fundamental constants, however, have been adopted from Ref. [81]. The corresponding results are summarized in the Table III, which is organized similarly to the Table II. Overall, the results shown in Table III confirm the findings obtained earlier. The relative smallness of the Coulomb-gauge many-potential contribution is illustrated by Fig. 9(a), where different contributions to the SE correction for the $1S_{1/2}$ state in both gauges are plotted as functions of Z . This smallness as well as the absence of cancellation between the momentum-space contributions in the Coulomb gauge is demonstrated also in Fig. 9(b), where the sum of the zero- and one-potential contributions is shown. For neon ($Z = 10$), a more "regular" behavior of the zero- and one-potential contributions in the Coulomb gauge is even more pronounced than for higher- Z systems. From Table III, it is seen that our results are in reasonable agreement with the results from Ref. [26]. We conclude that the most accurate calculations of the many-potential contributions can indeed be performed using the combination of the Coulomb gauge and the SC convergence-acceleration scheme.

Using the most effective methods among those examined, namely, the GF approach and the SC convergence-acceleration scheme, we consider the SE corrections for the $n = 2$ states: $2S_{1/2}$, $2P_{1/2}$, and $2P_{3/2}$. The SE corrections are calculated for hydrogen-like ions with $Z \in \{10, 18, 26, 36, 54, 82, 92, 100\}$. The corresponding results for both Feynman and Coulomb gauges are given in Table IV. Analyzing the table one can see that the accuracy of the total SE corrections for the excited states in hydrogen-like ions is still limited by the uncertainty of the many-potential contribution calculations. As in the case of the ground state, this contribution in the Coulomb gauge is significantly smaller than in the Feynman gauge. Moreover, the Coulomb gauge as before lacks strong cancellations between the momentum-space contributions. Finally, we note that our results are found to be in good agreement with the ones from Ref. [26].

V. CONCLUSION

The self-energy correction for various states of hydrogen-like ions is considered. Two gauges, Feynman and Coulomb ones, are studied, the acceleration tricks are discussed, and a self-consistent set of useful for the corresponding calculations formulas are collected.

The acceleration schemes do improve the accuracy of calculations. The combination of the Coulomb gauge and the Sapirstein-Cheng partial-wave-expansion convergence-acceleration scheme [73] is most suitable (among those considered) for calculating the self-energy correction in hydrogen-like ions, especially when studying light nuclei.

We believe that the analysis performed in the present work will facilitate the calculation of a wide range of more complex radiative corrections with the self-energy loop.

VI. ACKNOWLEDGMENTS

This work was supported by the Foundation for the Advancement of Theoretical Physics and Mathematics “BASIS”.

-
- [1] W. H. Furry, Phys. Rev. **81**, 115 (1951).
- [2] P. J. Mohr, G. Plunien, and G. Soff, Phys. Rep. **293**, 227 (1998).
- [3] V. A. Yerokhin, A. N. Artemyev, P. Indelicato, and V. M. Shabaev, Nucl. Instrum. Methods Phys. Res., Sect. B 11th International Conference on the Physics of Highly Charged Ions, **205**, 47 (2003).
- [4] J. Sapirstein and K. T. Cheng, Can. J. Phys. **86**, 25 (2008).
- [5] D. A. Glazov, Y. S. Kozhedub, A. V. Maiorova, V. M. Shabaev, I. I. Tupitsyn, A. V. Volotka, C. Kozhuharov, G. Plunien, and Th. Stöhlker, Hyp. Interact. **199**, 71 (2011).
- [6] A. V. Volotka, D. A. Glazov, G. Plunien, and V. M. Shabaev, Ann. Phys. (Berlin) **525**, 636 (2013).
- [7] V. M. Shabaev, A. I. Bondarev, D. A. Glazov, M. Y. Kaygorodov, Y. S. Kozhedub, I. A. Maltsev, A. V. Malyshev, R. V. Popov, I. I. Tupitsyn, and N. A. Zubova, Hyp. Interact. **239**, 60 (2018).
- [8] P. Indelicato, J. Phys. B: At. Mol. Opt. Phys. **52**, 232001 (2019).
- [9] V. M. Shabaev, in *Comprehensive Computational Chemistry (First Edition)*, edited by M. Yáñez and R. J. Boyd (Elsevier, Oxford, 2024) pp. 94–128.
- [10] U. D. Jentschura, P. J. Mohr, and G. Soff, Phys. Rev. Lett. **82**, 53 (1999).
- [11] V. A. Yerokhin and V. M. Shabaev, Phys. Rev. Lett. **115**, 233002 (2015).
- [12] V. A. Yerokhin, Z. Harman, and C. H. Keitel, Phys. Rev. Lett. **133**, 251803 (2024).
- [13] P. J. Mohr, D. B. Newell, B. N. Taylor, and E. Tiesinga, Rev. Mod. Phys. **97**, 025002 (2025).
- [14] W. Caswell and G. Lepage, Phys. Lett. B **167**, 437 (1986).
- [15] T. Stöhlker, P. H. Mokler, F. Bosch, R. W. Dunford, F. Franzke, O. Klepper, C. Kozhuharov, T. Ludziejewski, F. Nolden, H. Reich, P. Rymuza, Z. Stachura, M. Steck, P. Swiat, and A. Warczak, Phys. Rev. Lett. **85**, 3109 (2000).
- [16] A. Gumberidze, T. Stöhlker, D. Banaś, K. Beckert, P. Beller, H. F. Beyer, F. Bosch, S. Hagmann, C. Kozhuharov, D. Liesen, F. Nolden, X. Ma, P. H. Mokler, M. Steck, D. Sierpowski, and S. Tashenov, Phys. Rev. Lett. **94**, 223001 (2005).
- [17] J. Schweppe, A. Belkacem, L. Blumenfeld, N. Claytor, B. Feinberg, H. Gould, V. E. Kostroun, L. Levy, S. Misawa, J. R. Mowat, and M. H. Prior, Phys. Rev. Lett. **66**, 1434 (1991).
- [18] C. Brandau, C. Kozhuharov, A. Müller, W. Shi, S. Schippers, T. Bartsch, S. Böhm, C. Böhme, A. Hoffknecht, H. Knopp, N. Grün, W. Scheid, T. Steih, F. Bosch, B. Franzke, P. H. Mokler, F. Nolden, M. Steck, T. Stöhlker, and Z. Stachura, Phys. Rev. Lett. **91**, 073202 (2003).
- [19] P. Beiersdorfer, H. Chen, D. B. Thorn, and E. Träbert, Phys. Rev. Lett. **95**, 233003 (2005).
- [20] M. Trassinelli, A. Kumar, H. F. Beyer, P. Indelicato, R. Martin, R. Reuschl, Y. S. Kozhedub, C. Brandau, H. Bräuning, S. Geyer, A. Gumberidze, S. Hess, P. Jagodzinski, C. Kozhuharov, D. Liesen, U. Spillmann, S. Trotsenko, G. Weber, D. F. A. Winters, and T. Stöhlker, Europhys. Lett. **87**, 63001 (2009).
- [21] M. Trassinelli, A. Kumar, H. F. Beyer, P. Indelicato, R. Martin, R. Reuschl, Y. S. Kozhedub, C. Brandau, H. Bräuning, S. Geyer, A. Gumberidze, S. Hess, P. Jagodzinski, C. Kozhuharov, D. Liesen, U. Spillmann, S. Trotsenko, G. Weber, D. F. A. Winters, and T. Stöhlker, Phys. Scr. **2011**, 014003 (2011).
- [22] R. Loetzsch, H. F. Beyer, L. Duval, U. Spillmann, D. Banaś, P. Dergham, F. M. Kröger, J. Glorius, R. E. Grisenti, M. Guerra, A. Gumberidze, R. Heß, P.-M. Hillenbrand, P. Indelicato, P. Jagodzinski, E. Lamour, B. Lorentz, S. Litvinov, Y. A. Litvinov, J. Machado, N. Paul, G. G. Paulus, N. Petridis, J. P. Santos, M. Scheidel, R. S. Sidhu, M. Steck, S. Steydli, K. Szary, S. Trotsenko, I. Uschmann, G. Weber, T. Stöhlker, and M. Trassinelli, Nature **625**, 673 (2024).
- [23] V. A. Yerokhin, P. Indelicato, and V. M. Shabaev, Phys. Rev. Lett. **97**, 253004 (2006).
- [24] Y. S. Kozhedub, O. V. Andreev, V. M. Shabaev, I. I. Tupitsyn, C. Brandau, C. Kozhuharov, G. Plunien, and T. Stöhlker, Phys. Rev. A **77**, 032501 (2008).
- [25] J. Sapirstein and K. T. Cheng, Phys. Rev. A **83**, 012504 (2011).
- [26] V. A. Yerokhin and V. M. Shabaev, J. Phys. Chem. Ref. Data **44**, 033103 (2015).
- [27] A. N. Artemyev, V. M. Shabaev, V. A. Yerokhin, G. Plunien, and G. Soff, Phys. Rev. A **71**, 062104 (2005).
- [28] Y. S. Kozhedub, A. V. Malyshev, D. A. Glazov, V. M. Shabaev, and I. I. Tupitsyn, Phys. Rev. A **100**, 062506 (2019).
- [29] T. Beier, I. Lindgren, H. Persson, S. Salomonson, P. Sunnergren, H. Häfner, and N. Hermanspahn, Phys. Rev. A **62**, 032510 (2000).
- [30] V. A. Yerokhin, P. Indelicato, and V. M. Shabaev, Phys. Rev. Lett. **89**, 143001 (2002).
- [31] V. A. Yerokhin and V. M. Shabaev, Phys. Rev. A **64**, 012506 (2001).
- [32] J. Sapirstein and K. T. Cheng, Phys. Rev. A **63**, 032506 (2001).
- [33] V. A. Yerokhin and U. D. Jentschura, Phys. Rev. Lett. **100**, 163001 (2008).
- [34] V. A. Yerokhin and U. D. Jentschura, Phys. Rev. A **81**, 012502 (2010).
- [35] V. A. Agababaev, E. A. Prokhorchuk, D. A. Glazov, A. V. Malyshev, V. M. Shabaev, and A. V. Volotka, Phys. Rev. A **112**, 032818 (2025).
- [36] V. A. Yerokhin, K. Pachucki, Z. Harman, and C. H. Keitel, Phys. Rev. Lett. **107**, 043004 (2011).
- [37] V. A. Yerokhin, K. Pachucki, Z. Harman, and C. H. Keitel, Phys. Rev. A **85**, 022512 (2012).

- [38] M. G. Kozlov, V. A. Yerokhin, M. Y. Kaygorodov, and E. V. Tryapitsyna, *Phys. Rev. A* **110**, 062805 (2024).
- [39] A. V. Volotka, D. A. Glazov, G. Plunien, V. M. Shabaev, and I. I. Tupitsyn, *Eur. Phys. J. D* **38**, 293 (2006).
- [40] V. A. Yerokhin, A. N. Artemyev, and V. M. Shabaev, *Phys. Lett. A* **234**, 361 (1997).
- [41] H. Persson, I. Lindgren, L. N. Labzowsky, G. Plunien, T. Beier, and G. Soff, *Phys. Rev. A* **54**, 2805 (1996).
- [42] V. A. Yerokhin, A. N. Artemyev, T. Beier, G. Plunien, V. M. Shabaev, and G. Soff, *Phys. Rev. A* **60**, 3522 (1999).
- [43] A. V. Volotka, D. A. Glazov, V. M. Shabaev, I. I. Tupitsyn, and G. Plunien, *Phys. Rev. Lett.* **103**, 033005 (2009).
- [44] A. V. Volotka, D. A. Glazov, V. M. Shabaev, I. I. Tupitsyn, and G. Plunien, *Phys. Rev. Lett.* **112**, 253004 (2014).
- [45] P. J. Mohr, *Ann. Phys.* **88**, 26 (1974).
- [46] P. J. Mohr, *Ann. Phys.* **88**, 52 (1974).
- [47] G. Soff and P. J. Mohr, *Phys. Rev. A* **38**, 5066 (1988).
- [48] V. A. Yerokhin and A. V. Maiorova, *Symmetry* **12**, 800 (2020).
- [49] W. R. Johnson, S. A. Blundell, and J. Sapirstein, *Phys. Rev. A* **37**, 307 (1988).
- [50] I. I. Tupitsyn and A. V. Loginov, *Opt. Spectrosc.* **94**, 319 (2003).
- [51] S. Kotochigova, K. P. Kirby, and I. I. Tupitsyn, *Phys. Rev. A* **76**, 052513 (2007).
- [52] V. M. Shabaev, I. I. Tupitsyn, V. A. Yerokhin, G. Plunien, and G. Soff, *Phys. Rev. Lett.* **93**, 130405 (2004).
- [53] E. H. Wichmann and N. M. Kroll, *Phys. Rev.* **101**, 843 (1956).
- [54] J. Sapirstein and W. R. Johnson, *J. Phys. B* **29**, 5213 (1996).
- [55] W. R. Johnson, S. A. Blundell, and J. Sapirstein, *Phys. Rev. A* **37**, 307 (1988).
- [56] V. K. Ivanov, S. S. Baturin, D. A. Glazov, and A. V. Volotka, *Phys. Rev. A* **110**, 032815 (2024).
- [57] S. F. Boys and A. C. Egerton, *Proc. R. Soc. Lond. A* **200**, 542 (1950).
- [58] D. Ferenc, M. Salman, and T. Saue, “Gaussian basis set approach to one-loop self-energy,” (2025), arXiv:2501.10027 [quant-ph].
- [59] E. B. Rozenbaum, D. A. Glazov, V. M. Shabaev, K. E. Sosnova, and D. A. Telnov, *Phys. Rev. A* **89**, 012514 (2014).
- [60] A. N. Artemyev and A. Surzhykov, *Phys. Rev. Lett.* **114**, 243004 (2015).
- [61] DIRAC, a relativistic ab initio electronic structure program, Release DIRAC25 (2025), written by T. Saue, L. Visscher, H. J. Aa. Jensen, R. Bast and A. S. P. Gomes, with contributions from I. A. Aucar, V. Bakken, J. Brandejs, C. Chibueze, J. Creutzberg, K. G. Dyall, S. Dubillard, U. Ekström, E. Eliav, T. Enevoldsen, E. Faßhauer, T. Fleig, O. Fossgaard, K. G. Gaul, L. Halbert, E. D. Hedegård, T. Helgaker, B. Helmich-Paris, J. Henriksson, M. van Horn, M. Iliaš, Ch. R. Jacob, S. Knecht, S. Komorovský, O. Kullie, J. K. Lærdahl, C. V. Larsen, Y. S. Lee, N. H. List, H. S. Nataraj, M. K. Nayak, P. Norman, A. Nyvang, G. Olejniczak, J. Olsen, J. M. H. Olsen, A. Papadopoulos, Y. C. Park, J. K. Pedersen, M. Pernpointner, J. V. Pototschnig, R. di Remigio, M. Repisky, C. M. R. Rocha, K. Ruud, P. Salek, B. Schimmelpfennig, B. Senjean, A. Shee, J. Sikkema, A. Sunaga, A. J. Thorvaldsen, J. Thyssen, J. van Stralen, M. L. Vidal, S. Villaume, O. Visser, T. Winther, S. Yamamoto and X. Yuan (available at <https://doi.org/10.5281/zenodo.14833106>, see also <https://www.diracprogram.org>).
- [62] D. A. Glazov, A. V. Volotka, V. M. Shabaev, I. I. Tupitsyn, and G. Plunien, *Phys. Lett. A* **357**, 330 (2006).
- [63] N. J. Snyderman, *Ann. Phys.* **211**, 43 (1991).
- [64] P. J. Mohr, *Phys. Rev. A* **26**, 2338 (1982).
- [65] V. A. Yerokhin and V. M. Shabaev, *Phys. Rev. A* **60**, 800 (1999).
- [66] U. D. Jentschura, P. J. Mohr, and G. Soff, *Phys. Rev. A* **63**, 042512 (2001).
- [67] U. D. Jentschura and P. J. Mohr, *Phys. Rev. A* **69**, 064103 (2004).
- [68] V. A. Yerokhin and Z. Harman, *Phys. Rev. A* **95**, 060501 (2017).
- [69] D. Hedendahl and J. Holmberg, *Phys. Rev. A* **85**, 012514 (2012).
- [70] V. A. Yerokhin, Z. Harman, and C. H. Keitel, *Phys. Rev. A* **111**, 012802 (2025).
- [71] G. S. Adkins, *Phys. Rev. D* **47**, 3647 (1993).
- [72] V. A. Yerokhin and U. D. Jentschura, *Phys. Rev. A* **81**, 012502 (2010).
- [73] J. Sapirstein and K. T. Cheng, *Phys. Rev. A* **108**, 042804 (2023).
- [74] V. A. Yerokhin, K. Pachucki, and V. M. Shabaev, *Phys. Rev. A* **72**, 042502 (2005).
- [75] A. V. Malyshev, E. A. Prokhorchuk, and V. M. Shabaev, *Phys. Rev. A* **109**, 062802 (2024).
- [76] V. A. Yerokhin, Z. Harman, and C. H. Keitel, *Phys. Rev. A* **111**, 042820 (2025).
- [77] S. A. Blundell and N. J. Snyderman, *Phys. Rev. A* **44**, R1427 (1991).
- [78] A. N. Artemyev, V. M. Shabaev, I. I. Tupitsyn, G. Plunien, A. Surzhykov, and S. Fritzsche, *Phys. Rev. A* **88**, 032518 (2013).
- [79] A. N. Artemyev, V. M. Shabaev, I. I. Tupitsyn, G. Plunien, and V. A. Yerokhin, *Phys. Rev. Lett.* **98**, 173004 (2007).
- [80] J. Holmberg, *Phys. Rev. A* **84**, 062504 (2011).
- [81] E. Tiesinga, P. J. Mohr, D. B. Newell, and B. N. Taylor, *J. Phys. Chem. Ref. Data* **50**, 033105 (2021).
- [82] G. S. Adkins, *Phys. Rev. D* **27**, 1814 (1983).
- [83] J. Malenfant, *Phys. Rev. D* **35**, 1525 (1987).
- [84] D. A. Varshalovich, A. N. Moskalev, and V. K. Khersonskii, *Quantum Theory of Angular Momentum* (World Scientific, Singapore, 1988).
- [85] V. A. Yerokhin, C. H. Keitel, and Z. Harman, *Phys. Rev. A* **104**, 022814 (2021).

Table I. Contributions to the self-energy correction for the ground $1S_{1/2}$ state of hydrogen-like argon and uranium obtained in the Feynman (F) and Coulomb (C) gauges (in eV). The individual terms of the partial-wave expansion for the many-potential contribution as well as the results of applying the extrapolation procedure are shown. The nuclear-charge distribution is described by the homogeneously-charged-sphere model with the root-mean-square radii taken from Ref. [69].

	$Z = 18$		$Z = 92$	
	F	C	F	C
$\Delta\varepsilon_a^{0p}$	-67.924836	1.341667	-516.318629	210.068167
$\Delta\varepsilon_a^{1p}$	49.511442	0.054770	472.000467	213.738955
$\Delta\varepsilon_a^{\text{MP}}(k), k = 1$	18.954139	-0.098735	392.056752	-54.030900
2	0.447224	-0.044326	2.922927	-11.168699
3	0.115257	-0.011632	2.001276	-1.902586
4	0.046658	-0.006453	0.915478	-0.685643
5	0.023375	-0.004153	0.478148	-0.330469
6	0.013267	-0.002872	0.278392	-0.186004
7	0.008186	-0.002080	0.175634	-0.115450
8	0.005368	-0.001558	0.117699	-0.076706
9	0.003688	-0.001199	0.082646	-0.053600
10	0.002630	-0.000943	0.060225	-0.038946
11	0.001933	-0.000754	0.045228	-0.029195
12	0.001458	-0.000613	0.034822	-0.022452
13	0.001124	-0.000505	0.027378	-0.017638
14	0.000882	-0.000420	0.021913	-0.014110
15	0.000704	-0.000353	0.017811	-0.011464
16	0.000570	-0.000300	0.014672	-0.009441
17	0.000468	-0.000257	0.012229	-0.007868
18	0.000388	-0.000221	0.010300	-0.006626
19	0.000325	-0.000192	0.008756	-0.005632
20	0.000275	-0.000168	0.007506	-0.004827
21	0.000234	-0.000147	0.006483	-0.004169
22	0.000201	-0.000130	0.005638	-0.003625
23	0.000174	-0.000115	0.004933	-0.003172
24	0.000152	-0.000103	0.004341	-0.002792
$\sum_{k=1}^{24}$	19.628680	-0.178229	399.311187	-68.732014
$\sum_{k=25}^{\infty}$ [extr.]	0.001595(16)	-0.001300(15)	0.049936(33)	-0.032109(30)
$\Delta\varepsilon_a$	1.216893(16)	1.216897(15)	355.042972(33)	355.042991(30)

Table II. Individual contributions to the self-energy correction for the $1S_{1/2}$ state of hydrogen-like ions in the Feynman (F) and Coulomb (C) gauges (in eV). The many-potential contribution is calculated in three ways: directly (DIR), using the two-potential (TP) scheme, and using the Sapirstein-Cheng (SC) approach. The nuclear-charge distribution is described by the homogeneously-charged-sphere model with the root-mean-square radii taken from Ref. [69]. The values of fundamental constants are adopted from the same Ref. [69].

Z	Gauge	$\Delta\epsilon_a^{0p}$	$\Delta\epsilon_a^{1p}$	Scheme	Method	$\Delta\epsilon_a^{2p} / \Delta\tilde{\epsilon}_a^{2p}$	$\Delta\epsilon_a^{(3+)p} / \Delta\tilde{\epsilon}_a^{(3+)p}$	$\Delta\epsilon_a^{Mp}$	$\Delta\epsilon_a$
18	F	-67.924 836 710	49.511 442 330	DIR	DKB	-	-	19.629 9(55)	1.216 5(55)
				DIR	GF	-	-	19.630 288(16)	1.216 893(16)
				TP	GF	8.960 544 0(13)	10.669 757 05(68)	19.630 301 0(15)	1.216 906 6(15)
				SC	DKB	8.722 252 397	10.908 04(23)	19.630 29(23)	1.216 90(23)
				SC	GF		10.908 049 07(50)	19.630 301 47(50)	1.216 907 09(50)
	Ref. [69]	-67.924 837 74(5)	49.511 443 05(6)	DIR		-	-	19.630 296(10)	1.216 90(1)
	C	1.341 667 275	0.054 770 246	DIR	DKB	-	-	-0.179 54(29)	1.216 89(29)
				DIR	GF	-	-	-0.179 540(15)	1.216 898(15)
				TP	GF	-0.155 550 76(88)	-0.023 979 87(14)	-0.179 530 63(89)	1.216 906 89(89)
				SC	DKB	-0.218 341 867	0.038 78(12)	-0.179 56(12)	1.216 88(12)
SC				GF		0.038 811 53(20)	-0.179 530 33(20)	1.216 907 19(20)	
Ref. [69]	1.341 668 068(1)	0.054 770 997(7)	DIR		-	-	-0.179 538(3)	1.216 901(3)	
54	F	-285.092 638 464	190.356 023 847	DIR	DKB	-	-	145.735 9(42)	50.999 3(42)
				DIR	GF	-	-	145.733 863(48)	50.997 249(48)
				TP	GF	55.334 247 42(67)	90.399 626 4(62)	145.733 873 8(62)	50.997 259 2(62)
				SC	DKB	54.420 120 868	91.312 5(14)	145.732 7(14)	50.996 0(14)
				SC	GF		91.313 752 7(60)	145.733 873 6(60)	50.997 259 0(60)
	Ref. [69]	-285.092 638 6(1)	190.356 052 0(3)	DIR		-	-	145.733 90(8)	50.997 31(8)
	C	43.590 610 210	17.387 958 323	DIR	DKB	-	-	-9.979 4(45)	50.999 2(45)
				DIR	GF	-	-	-9.981 316(33)	50.997 253(33)
				TP	GF	-6.727 056 81(91)	-3.254 252 0(41)	-9.981 308 8(42)	50.997 259 7(42)
				SC	DKB	-7.403 692 141	-2.577 71(19)	-9.981 41(19)	50.997 16(19)
SC				GF		-2.577 617 0(22)	-9.981 309 1(22)	50.997 259 4(22)	
Ref. [69]	43.590 621 48(6)	17.387 986 7(3)	DIR		-	-	-9.981 343(16)	50.997 27(2)	
92	F	-516.318 629 247	472.000 467 757	DIR	DKB	-	-	399.41(10)	355.09(10)
				DIR	GF	-	-	399.361 134(33)	355.042 972(33)
				TP	GF	144.424 321(12)	254.936 813(21)	399.361 134(24)	355.042 972(24)
				SC	DKB	149.189 230 301	250.22(11)	399.41(11)	355.09(11)
				SC	GF		250.171 906(27)	399.361 136(27)	355.042 975(27)
	Ref. [69]	-516.318 598(4)	472.000 597(6)	DIR		-	-	399.361 2(2)	355.043 2(2)
	C	210.068 167 293	213.738 955 307	DIR	DKB	-	-	-68.807(81)	355.000(81)
				DIR	GF	-	-	-68.764 132(30)	355.042 991(30)
				TP	GF	-31.829 252(29)	-36.934 880 2(21)	-68.764 132(29)	355.042 991(29)
				SC	DKB	-23.349 279 138	-45.463(84)	-68.812(84)	354.995(84)
SC				GF		-45.414 864 2(36)	-68.764 143 3(36)	355.042 979 3(36)	
Ref. [69]	210.068 220 5(7)	213.739 094(4)	DIR		-	-	-68.764 3(1)	355.043 0(1)	

Table III. Self-energy, $1S_{1/2}$ state (*continued*).

Z	Gauge	$\Delta\varepsilon_a^{0p}$	$\Delta\varepsilon_a^{1p}$	Scheme	Method	$\Delta\varepsilon_a^{2p} / \Delta\varepsilon_a^{2p}$	$\Delta\varepsilon_a^{(3+)p} / \Delta\varepsilon_a^{(3+)p}$	$\Delta\varepsilon_a^{Mp}$	$\Delta\varepsilon_a$
54	F	-9.961 275 619	6.651 147 516	DIR	DKB	-	-	5.092 05(49)	1.781 92(49)
				DIR	GF	-	-	5.092 013 7(53)	1.781 885 6(53)
				TP	GF	1.933 405 159(24)	3.158 609 71(91)	5.092 014 87(91)	1.781 886 77(91)
				SC	DKB	1.901 467 097	3.190 533(21)	5.092 000(21)	1.781 872(21)
				SC	GF		3.190 547 78(77)	5.092 014 87(77)	1.781 886 77(77)
	Ref. [26]							1.781 887(2)(2)	
	C	1.523 080 462	0.607 564 155	DIR	DKB	-	-	-0.348 739(67)	1.781 906(67)
				DIR	GF	-	-	-0.348 758 6(38)	1.781 886 0(38)
				TP	GF	-0.235 050 090(32)	-0.113 707 65(47)	-0.348 757 74(47)	1.781 886 88(47)
				SC	DKB	-0.258 689 306	-0.090 087(20)	-0.348 777(20)	1.781 868(20)
SC				GF		-0.090 068 48(27)	-0.348 757 78(27)	1.781 886 83(27)	
Ref. [26]							1.781 887(2)(2)		
82	F	-2.952 357 937	2.371 873 437	DIR	DKB	-	-	2.067 807(47)	1.487 323(47)
				DIR	GF	-	-	2.067 770 05(56)	1.487 285 55(56)
				TP	GF	0.738 029 090 8(61)	1.329 741 01(32)	2.067 770 10(32)	1.487 285 60(32)
				SC	DKB	0.745 897 727	1.321 869(19)	2.067 766(19)	1.487 282(19)
				SC	GF		1.321 872 37(33)	2.067 770 10(33)	1.487 285 60(33)
	Ref. [26]							1.487 286(16)(3)	
	C	0.994 837 254	0.787 437 130	DIR	DKB	-	-	-0.294 96(11)	1.487 31(11)
				DIR	GF	-	-	-0.294 988 82(36)	1.487 285 57(36)
				TP	GF	-0.153 987 847(36)	-0.141 000 92(20)	-0.294 988 77(20)	1.487 285 61(20)
				SC	DKB	-0.132 956 055	-0.162 040(11)	-0.294 996(11)	1.487 278(11)
SC				GF		-0.162 032 73(14)	-0.294 988 78(14)	1.487 285 60(14)	
Ref. [26]							1.487 286(16)(3)		
92	F	-2.141 311 301	1.957 559 518	DIR	DKB	-	-	1.656 244(75)	1.472 492(75)
				DIR	GF	-	-	1.656 240 14(29)	1.472 488 36(29)
				TP	GF	0.598 961 340 3(33)	1.057 278 83(17)	1.656 240 17(17)	1.472 488 39(17)
				SC	DKB	0.618 726 402	1.037 484(40)	1.656 210(40)	1.472 458(40)
				SC	GF		1.037 513 75(23)	1.656 240 16(23)	1.472 488 37(23)
	Ref. [26]							1.472 50(1)(2)	
	C	0.871 179 702	0.886 500 900	DIR	DKB	-	-	-0.285 190 5(40)	1.472 490 1(40)
				DIR	GF	-	-	-0.285 192 06(32)	1.472 488 54(32)
				TP	GF	-0.132 008 642(12)	-0.153 183 501(35)	-0.285 192 142(37)	1.472 488 460(37)
				SC	DKB	-0.096 833 870	-0.188 360(17)	-0.285 194(17)	1.472 487(17)
SC				GF		-0.188 358 295(21)	-0.285 192 165(21)	1.472 488 437(21)	
Ref. [26]							1.472 50(1)(2)		
100	F	-1.737 050 769	1.795 888 856	DIR	GF	-	-	1.437 300 86(13)	1.496 138 95(13)
				TP	GF	0.534 332 311	0.902 968 55(10)	1.437 300 86(10)	1.496 138 94(10)
				SC	GF	0.565 473 422	0.871 827 40(16)	1.437 300 82(16)	1.496 138 91(16)
	Ref. [26]							1.496 14(7)(47)	
	C	0.780 926 903	0.996 469 025	DIR	GF	-	-	-0.281 256 83(39)	1.496 139 10(39)
				TP	GF	-0.116 019 006(13)	-0.165 237 923(60)	-0.281 256 929(62)	1.496 138 999(62)
				SC	GF	-0.068 173 067	-0.213 083 879(35)	-0.281 256 946(35)	1.496 138 982(35)
	Ref. [26]							1.496 14(7)(47)	

Table IV: Contributions to the self-energy corrections for the $2S_{1/2}$, $2P_{1/2}$, and $2P_{3/2}$ states of hydrogen-like ions. Results are given in terms of the dimensionless function $F(\alpha Z)$ defined in Eq. (50). For $Z = 10$, the homogeneously-charged-sphere model is used, while for other values of Z the Fermi model is used. Nuclear root-mean-square radii are taken from Ref. [26]. The values of fundamental constants are adopted from Ref. [81]. The many-potential contribution is obtained within the Sapirstein-Cheng convergence-acceleration scheme.

Z	Gauge		$2S_{1/2}$	$2P_{1/2}$	$2P_{3/2}$
10	F	$\Delta\varepsilon_a^{0P}$	-2 075.579 237 771	-2 196.693 661 912	-2 192.070 770 920
		$\Delta\varepsilon_a^{1P}$	1 719.050 474 880	1 818.840 183 393	1 815.473 220 245
		$\Delta\varepsilon_a^{MP}$	361.423 177(95)	377.738 68(14)	376.727 908(77)
		$\Delta\varepsilon_a$	4.894 415(95)	-0.114 80(14)	0.130 358(77)
	C	$\Delta\varepsilon_a^{0P}$	7.190 429 621	2.624 890 307	2.775 883 599
		$\Delta\varepsilon_a^{1P}$	-1.534 430 545	-2.119 896 459	-2.038 942 518
		$\Delta\varepsilon_a^{MP}$	-0.761 608(15)	-0.619 823(41)	-0.606 587 0(90)
		$\Delta\varepsilon_a$	4.894 391(15)	-0.114 829(41)	0.130 354 0(90)
		$\Delta\varepsilon_a$, [26]	4.894 384(7)	-0.114 84(2)	0.130 36(2)
18	F	$\Delta\varepsilon_a^{0P}$	-510.933 712 531	-547.071 566 494	-543.528 241 119
		$\Delta\varepsilon_a^{1P}$	405.527 774 766	431.854 905 602	429.503 304 379
		$\Delta\varepsilon_a^{MP}$	109.105 831(51)	115.119 152(77)	114.165 747(15)
		$\Delta\varepsilon_a$	3.699 893(51)	-0.097 509(77)	0.140 810(15)
	C	$\Delta\varepsilon_a^{0P}$	5.135 244 411	2.027 253 175	2.157 952 816
		$\Delta\varepsilon_a^{1P}$	-0.736 198 502	-1.519 146 727	-1.443 991 645
		$\Delta\varepsilon_a^{MP}$	-0.699 151(12)	-0.605 613(34)	-0.573 141 2(22)
		$\Delta\varepsilon_a$	3.699 895(12)	-0.097 507(34)	0.140 819 9(22)
		$\Delta\varepsilon_a$, [26]	3.699 892	-0.097 511(4)	0.140 819
26	F	$\Delta\varepsilon_a^{0P}$	-207.664 305 943	-224.482 210 414	-221.561 948 805
		$\Delta\varepsilon_a^{1P}$	159.521 301 465	169.968 233 475	168.173 153 568
		$\Delta\varepsilon_a^{MP}$	51.202 289(18)	54.437 750(31)	53.542 405(15)
		$\Delta\varepsilon_a$	3.059 284(18)	-0.076 227(31)	0.153 610(15)
	C	$\Delta\varepsilon_a^{0P}$	4.030 422 889	1.681 608 238	1.790 274 523
		$\Delta\varepsilon_a^{1P}$	-0.321 172 956	-1.166 082 251	-1.100 585 293
		$\Delta\varepsilon_a^{MP}$	-0.649 958 1(65)	-0.591 744(19)	-0.536 070 7(33)
		$\Delta\varepsilon_a$	3.059 291 9(65)	-0.076 218(19)	0.153 618 5(33)
		$\Delta\varepsilon_a$, [26]	3.059 292(1)	-0.076 218(1)	0.153 620
36	F	$\Delta\varepsilon_a^{0P}$	-92.012 084 971	-100.545 376 092	-98.122 650 921
		$\Delta\varepsilon_a^{1P}$	68.478 913 119	72.554 183 239	71.176 248 946
		$\Delta\varepsilon_a^{MP}$	26.118 135(10)	27.946 190(13)	27.118 204(15)
		$\Delta\varepsilon_a$	2.584 964(10)	-0.045 003(13)	0.171 802(15)
	C	$\Delta\varepsilon_a^{0P}$	3.191 617 572	1.402 984 217	1.483 773 405
		$\Delta\varepsilon_a^{1P}$	-0.003 718 984	-0.871 022 395	-0.823 673 062
		$\Delta\varepsilon_a^{MP}$	-0.602 927 7(25)	-0.576 955 6(70)	-0.488 293 4(27)
		$\Delta\varepsilon_a$	2.584 970 9(25)	-0.044 993 8(70)	0.171 806 9(27)
		$\Delta\varepsilon_a$, [26]	2.584 972	-0.044 991	0.171 808

Table IV: Self-energy, excited states (*continued*).

Z	Gauge		$2S_{1/2}$	$2P_{1/2}$	$2P_{3/2}$
54	F	$\Delta\varepsilon_a^{0P}$	-32.616 716 171	-36.324 811 900	-34.414 650 841
		$\Delta\varepsilon_a^{1P}$	23.445 352 616	24.194 742 894	23.197 273 689
		$\Delta\varepsilon_a^{MP}$	11.331 970(13)	12.155 676(19)	11.425 938 1(82)
		$\Delta\varepsilon_a$	2.160 606(13)	0.025 607(19)	0.208 560 9(82)
	C	$\Delta\varepsilon_a^{0P}$	2.346 175 319	1.103 617 134	1.136 073 664
		$\Delta\varepsilon_a^{1P}$	0.361 787 949	-0.516 470 137	-0.523 758 607
		$\Delta\varepsilon_a^{MP}$	-0.547 352 6(17)	-0.561 533 9(54)	-0.403 752 2(13)
		$\Delta\varepsilon_a$	2.160 610 7(17)	0.025 613 1(54)	0.208 562 9(13)
		$\Delta\varepsilon_a$, [26]	2.160 612(2)(3)	0.025 617	0.208 563
82	F	$\Delta\varepsilon_a^{0P}$	-11.119 815 486	-12.768 564 627	-11.152 418 631
		$\Delta\varepsilon_a^{1P}$	8.151 898 860	7.689 867 435	6.797 162 744
		$\Delta\varepsilon_a^{MP}$	5.033 280 8(93)	5.284 306(16)	4.626 975 8(34)
		$\Delta\varepsilon_a$	2.065 364 2(93)	0.205 609(16)	0.271 719 9(34)
	C	$\Delta\varepsilon_a^{0P}$	1.703 650 832	0.860 750 394	0.829 247 308
		$\Delta\varepsilon_a^{1P}$	0.875 870 907	-0.073 015 197	-0.274 656 464
		$\Delta\varepsilon_a^{MP}$	-0.514 155 8(23)	-0.582 123 8(57)	-0.282 870 37(79)
		$\Delta\varepsilon_a$	2.065 365 9(23)	0.205 611 4(57)	0.271 720 47(79)
		$\Delta\varepsilon_a$, [26]	2.065 367(23)(5)	0.205 613(1)(0)	0.271 721
92	F	$\Delta\varepsilon_a^{0P}$	-8.389 628 927	-9.729 683 232	-8.095 704 176
		$\Delta\varepsilon_a^{1P}$	6.410 146 198	5.762 419 098	4.775 608 621
		$\Delta\varepsilon_a^{MP}$	4.149 985 9(48)	4.284 126 6(80)	3.615 136 6(45)
		$\Delta\varepsilon_a$	2.170 503 2(48)	0.316 862 5(80)	0.295 041 1(45)
	C	$\Delta\varepsilon_a^{0P}$	1.553 629 935	0.800 352 700	0.755 392 208
		$\Delta\varepsilon_a^{1P}$	1.134 051 703	0.128 027 677	-0.216 677 107
		$\Delta\varepsilon_a^{MP}$	-0.517 176 60(74)	-0.611 515 3(27)	-0.243 672 49(13)
		$\Delta\varepsilon_a$	2.170 505 03(74)	0.316 865 1(27)	0.295 042 61(13)
		$\Delta\varepsilon_a$, [26]	2.170 52(2)(2)	0.316 869(2)(2)	0.295 043(0)(1)
100	F	$\Delta\varepsilon_a^{0P}$	-6.953 875 290	-8.114 515 401	-6.400 104 490
		$\Delta\varepsilon_a^{1P}$	5.597 189 494	4.824 500 696	3.682 814 800
		$\Delta\varepsilon_a^{MP}$	3.681 360 3(44)	3.735 025 9(74)	3.030 820 0(39)
		$\Delta\varepsilon_a$	2.324 674 5(44)	0.445 011 2(74)	0.313 530 4(39)
	C	$\Delta\varepsilon_a^{0P}$	1.438 749 738	0.749 905 361	0.704 955 752
		$\Delta\varepsilon_a^{1P}$	1.413 259 460	0.344 771 111	-0.177 247 595
		$\Delta\varepsilon_a^{MP}$	-0.527 333 13(74)	-0.649 663 0(26)	-0.214 176 47(12)
		$\Delta\varepsilon_a$	2.324 676 06(74)	0.445 013 4(26)	0.313 531 68(12)
		$\Delta\varepsilon_a$, [26]	2.324 7(1)(8)	0.445 01(1)(9)	0.313 53(0)(2)

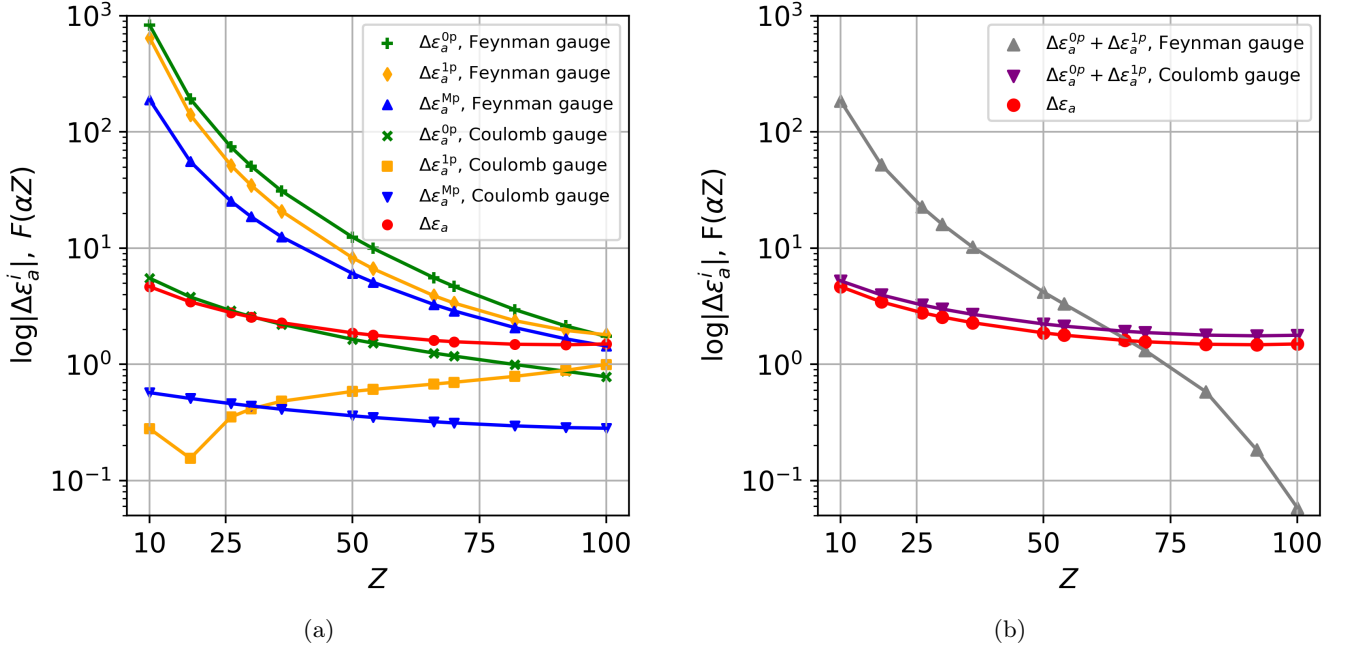


Figure 9. Individual contributions in two gauges to the self-energy correction for the $1S_{1/2}$ state (in terms of dimensionless function $F(\alpha Z)$ defined in Eq. (50)) as a function of the nuclear charge Z . The zero-, one-, and many-potential contributions are shown in Fig. 9(a). Sums of zero- and one-potential contributions are shown in Fig. 9(b). The total self-energy corrections, which are gauge-independent, are shown in both graphs. Note that for negative values their absolute values are taken. For convenience, the markers are connected with straight lines.

Appendix A: Free-electron self-energy operator

We define the free-electron self-energy operator as:

$$\Sigma^{(0)}(\mathbf{p}) = 4\pi\alpha i \int \frac{d^4\mathbf{k}}{(2\pi)^4} \gamma^\mu \frac{\not{\mathbf{p}} - \not{\mathbf{k}} + m_e}{(\mathbf{p} - \mathbf{k})^2 - m_e^2 + i0} \gamma^\nu D_{\mu\nu}(\mathbf{k}), \quad (\text{A1})$$

where $\not{\mathbf{p}} = \mathbf{p}_\mu \gamma^\mu$ and the photon propagator $D_{\mu\nu}$ is

$$D_{\mu\nu}^F(\mathbf{k}) = -\frac{g_{\mu\nu}}{\mathbf{k}^2} \quad (\text{A2})$$

in the Feynman gauge and

$$D_{\mu\nu}^C(\mathbf{k}) = \frac{1}{\mathbf{k}^2} \left(-g_{\mu\nu} - \frac{k_\mu k_\nu}{\mathbf{k}^2} + \frac{k^0(k_\mu \delta_{\nu 0} + k_\nu \delta_{\mu 0})}{\mathbf{k}^2} \right) \quad (\text{A3})$$

in the Coulomb gauge. In Eq. (A3), $\delta_{\nu\mu}$ is the four-dimensional Kronecker delta, $\delta_{\mu\nu} \equiv \delta_\mu^\nu$. The expression (A1) is UV divergent in both gauges. To eliminate the UV divergences, we apply the renormalization procedure. To make sense of divergent expressions, we use the dimensional regularization $d = 4 - 2\varepsilon$. In both gauges, we separate out the UV divergent part by writing the self-energy in the form:

$$\Sigma^{(0)}(\mathbf{p}) = \delta m - \frac{\alpha}{4\pi} \Delta_\varepsilon (\not{\mathbf{p}} - m_e) + \Sigma_R^{(0)}(\mathbf{p}), \quad (\text{A4})$$

where $\Delta_\varepsilon = 1/\varepsilon - \gamma_E + \ln 4\pi + \ln m_e$, γ_E is the Euler constant, and the mass counterterm is

$$\delta m = \frac{3\alpha}{4\pi} m_e \left(\Delta_\varepsilon + \frac{4}{3} \right). \quad (\text{A5})$$

Note that following Ref. [65] we use this definition of $\Sigma_R^{(0)}$ instead of writing a more familiar expression in terms of the renormalization constant Z_2 . In the Feynman gauge, the second approach leads to the IR singularities of individual contributions. In the Coulomb gauge, both approaches are equally convenient, but, for consistency, we write the expression for the free-electron self-energy operator in this form.

The renormalized part of the free-electron self-energy operator on the right-hand side of Eq. (A4) can be written in the form:

$$\Sigma_R^{(0)}(\mathbf{p}) = \frac{\alpha}{4\pi} (a(p_0, p) + \not{p}b(p_0, p) + \gamma^0 c(p_0, p)). \quad (\text{A6})$$

The coefficients a , b and c are gauge-dependent. In the Feynman gauge, they can be found, e.g., in Ref. [65]:

$$\begin{aligned} a(p_0, p) &= 2m_e \left(1 + \frac{2\rho}{1-\rho} \ln \rho \right), \\ b(p_0, p) &= -\frac{2-\rho}{1-\rho} \left(1 + \frac{\rho}{1-\rho} \ln \rho \right), \\ c(p_0, p) &= 0, \end{aligned} \quad (\text{A7})$$

where $\rho = 1 - \mathbf{p}^2/m_e^2$. For the Coulomb gauge, they could be derived from the expression obtained in Ref. [82]:

$$\begin{aligned} \Sigma^{(0)}(\mathbf{p}) &= \frac{\alpha m_e}{4\pi} (3\Delta_\varepsilon + 4) - \delta m - \frac{\alpha}{4\pi} \Delta_\varepsilon (\not{p} - m_e) + \frac{\alpha}{4\pi} \left(\frac{19}{6} (\boldsymbol{\gamma} \cdot \mathbf{p}) - \frac{1}{2} \gamma^0 p_0 \right. \\ &\quad \left. - \int_0^1 \frac{dx}{\sqrt{x}} \ln X [(1-x)(\mathbf{p} \cdot \boldsymbol{\gamma}) + m_e] + 2 \int_0^1 dx \ln Y [(1-x)\not{p} - m_e] + 2(\boldsymbol{\gamma} \cdot \mathbf{p}) \int_0^1 dx du \sqrt{x} \ln Z \right), \end{aligned} \quad (\text{A8})$$

where

$$\begin{aligned} X &= 1 + \frac{p^2}{m_e^2} (1-x), \\ Y &= 1 - \frac{p^2}{m_e^2} (1-x) - i0, \\ Z &= 1 - \frac{p_0^2}{m_e^2} (1-u) + \frac{p^2}{m_e^2} (1-xu) - i0. \end{aligned} \quad (\text{A9})$$

Some integrals in these expressions can be evaluated analytically, which was done, e.g., in Ref. [83]. The latter results allows one to write for the coefficients a , b , and c :

$$\begin{aligned} a(p_0, p) &= 2m_e \left(1 - F_0 + \frac{\rho \log \rho}{1-\rho} \right), \\ b(p_0, p) &= \frac{(\rho-2)(1-\rho+\rho \ln \rho)}{(1-\rho)^2} - 2F_2 \rho + \frac{2m_e^2 (F_1 \rho \ln \rho - F_0)}{p^2}, \\ c(p_0, p) &= 2\frac{p_0}{p^2} (F_0 m_e^2 - F_1 m_e^2 \rho \ln \rho + F_2 \rho p^2), \end{aligned} \quad (\text{A10})$$

where F_0 , F_1 , and F_2 are defined according to

$$\begin{aligned} F_0 &= \frac{\sqrt{p^2 + m_e^2}}{p} \ln \left| \frac{\sqrt{p^2 + m_e^2} + p}{\sqrt{p^2 + m_e^2} - p} \right| - 2, \\ F_1 &= \frac{p_0}{p} \ln \left| \frac{p_0 + p}{p_0 - p} \right| - 2, \\ F_2 &= \int_0^1 dx \frac{\sqrt{x} \ln X}{X - \rho + i0}. \end{aligned} \quad (\text{A11})$$

Appendix B: Free-electron vertex operator

In order to calculate the one-potential term, one needs the free-electron vertex function given by:

$$\Gamma^\mu(\mathbf{p}', \mathbf{p}) = 4\pi\alpha i \int \frac{d^4\mathbf{k}}{(2\pi)^4} \gamma^\sigma \frac{\not{p}' - \not{\mathbf{k}} + m_e}{(\mathbf{p}' - \mathbf{k})^2 - m_e^2} \gamma^\mu \frac{\not{p} - \not{\mathbf{k}} + m_e}{(\mathbf{p} - \mathbf{k})^2 - m_e^2} \gamma^\rho D_{\sigma\rho}(\mathbf{k}). \quad (\text{B1})$$

This expression is UV divergent in both gauges. Using dimensional regularization, it can be written as:

$$\Gamma^\mu(\mathbf{p}', \mathbf{p}) = \frac{\alpha}{4\pi} \Delta_\varepsilon \gamma^\mu + \Gamma_R^\mu(\mathbf{p}', \mathbf{p}), \quad (\text{B2})$$

where, as in the case of the free-electron self-energy operator, the UV finite part of Γ_R also turns out to be IR finite. For brevity, we discuss below only the time component of the operator, Γ_R^0 , for the case when $p_0 = p'_0 = \varepsilon_a$:

$$\begin{aligned} \Gamma_R^0(\mathbf{p}', \mathbf{p}) = \frac{\alpha}{4\pi} \{ & A\gamma^0 + \not{\mathbf{p}}'(B_1 + B_2)\varepsilon_a + \not{\mathbf{p}}(C_1 + C_2)\varepsilon_a + D(\not{\mathbf{p}}'\gamma^0\not{\mathbf{p}}) \\ & + (H_1 + H_2)\varepsilon_a + G_1\not{\mathbf{p}}'\gamma^0 + G_2\not{\mathbf{p}}\gamma^0 \}. \end{aligned} \quad (\text{B3})$$

In the Feynman gauge:

$$\begin{aligned} A &= C_5 - 2 + \mathbf{p}'^2 C_{11} + \mathbf{p}^2 C_{12} + 4(\mathbf{p}' \cdot \mathbf{p})(C_{00} + C_{11} + C_{12}) + m_e^2(-2C_{00} + C_{11} + C_{12}), \\ B_1 &= -4(C_{11} + C_{23}), \quad B_2 = -4(C_{00} + C_{11} + C_{12} + C_{25}), \\ C_1 &= B_2, \quad C_2 = -4(C_{12} + C_{24}), \\ D &= 2(C_{00} + C_{11} + C_{12}), \\ H_1 &= 4m_e(C_{00} + 2C_{11}), \quad H_2 = 4m_e(C_{00} + 2C_{12}), \quad G_1 = G_2 = 0, \end{aligned} \quad (\text{B4})$$

where

$$\begin{aligned} C_{ij} &= \int_0^1 \frac{dy}{(y\mathbf{p}' + (1-y)\mathbf{p})^2} S_i K_j, \\ S_{0,1,2} &= \{-\ln X', 1 - Y' \ln X', -\frac{1}{2} + Y' - Y'^2 \ln X'\}, \\ K_{0,1,2,3,4,5} &= \{1, y, 1 - y, y^2, (1 - y)^2, y(1 - y)\}, \\ C_5 &= -\int_0^1 dy \ln(y^2 k^2 / m_e^2 - y k^2 / m_e^2 + 1), \\ X' &= 1 + \frac{1}{Y'}, \quad Y' = \frac{m_e^2 - y\mathbf{p}'^2 - (1 - y)\mathbf{p}^2}{(y\mathbf{p}' + (1 - y)\mathbf{p})^2}, \end{aligned} \quad (\text{B5})$$

and $\mathbf{k} = \mathbf{p} - \mathbf{p}'$. For the Coulomb gauge, these coefficients can be readily determined from Ref. [80]:

$$\begin{aligned} B_1 &= F_{19} - F_{20} + 4(F_5 - F_3) + 2p'^2(F_{14} - 2F_{17}) + \\ &+ 2p^2(F_{13} - F_{14} - 2F_{16} + 2F_{17}) + 2(\mathbf{p}' \cdot \mathbf{p})(F_{13} - F_{16}), \\ C_1 &= F_{19} - F_{20} + 4(F_3 - F_2 + F_4 - F_5) + \\ &+ 2p'^2(F_{13} - F_{14} - F_{16} + F_{17}) + \\ &+ 2p^2(F_{12} - 2F_{13} + F_{14} - F_{15} + 2F_{16} - F_{17}) + \\ &+ 2(\mathbf{p}' \cdot \mathbf{p})(F_{12} - F_{13} - F_{15} + F_{16}), \\ D &= F_7 - F_{10} + 2(F_{19} - F_1) + \\ &+ 2p^2(F_{12} - 2F_{13}) + 4F_{13}(\mathbf{p}' \cdot \mathbf{p}) + 2k^2 F_{14}, \\ B_2 &= C_2 = -D, \\ G_1 &= m_e[F_{10} - F_{19} + 2p^2 F_{13} - 2(\mathbf{p}' \cdot \mathbf{p})F_{13} - 2k^2 F_{14}], \\ G_2 &= m_e[F_{10} - F_{19} + 2p^2(F_{13} - F_{12}) + 2(\mathbf{p}' \cdot \mathbf{p})(F_{12} - F_{13}) + 2k^2(F_{13} - F_{14})], \\ H_1 &= 4m_e(F_2 - F_1), \\ H_2 &= -G_1 - G_2, \end{aligned} \quad (\text{B6})$$

and finally A :

$$\begin{aligned} A &= \varepsilon_a^2(2F_1 - F_2) - F_{22} + m_e^2(2F_1 - 3F_2) + p'^2(F_{11} - F_8 + 4F_5 - 5F_3) - \\ &- 4(\mathbf{p}' \cdot \mathbf{p})^2 F_{13} + p^2(F_{10} - F_{11} - 5F_2 + 5F_3 + 4F_4 - 4F_5 - F_7 + \\ &+ F_8 + (\mathbf{p}' \cdot \mathbf{p})(-2F_{12} + 4F_{13})) + (-4F_5 + 4F_6 + 2F_8 - 2F_9)k^2 + \\ &+ (\mathbf{p}' \cdot \mathbf{p})(4F_1 - 2F_{19} - 2F_2 - 2F_{14}k^2) - \varepsilon_a^2(B_1 + C_1 - D). \end{aligned} \quad (\text{B7})$$

The coefficients F_{1-22} introduced above can be determined as follows. Let us define $B_{i,j}^k$ as

$$B_{i,j}^k = \begin{cases} 1, & \text{if } i \leq k \leq j, \\ 0, & \text{otherwise.} \end{cases} \quad (\text{B8})$$

then for $F_1 - F_6$ one obtains

$$\begin{aligned} F_i &= \int_0^1 \frac{du}{t^2} \left[C_1^i \delta_1 + C_2^i - C_3^i \frac{A}{t^2} \right] C_4^i, \\ \delta_1 &= \ln \left(\frac{t^2 + A}{A} \right), \quad C_1^i = \left[1 - B_{2,6}^i \left(1 + \frac{A}{t^2} \right) \right] \left[1 - B_{4,6}^i \left(1 + \frac{A}{t^2} \right) \right], \\ C_2^i &= B_{2,3}^i + \frac{1}{2} B_{4,6}^i, \quad C_3^i = B_{4,6}^i, \quad C_4^i = \{1, 1, u, 1, u, u^2\}. \end{aligned} \quad (\text{B9})$$

Here, $A = m_e^2 - up^2 - (1-u)p^2$, $t = up' + (1-u)p$. For F_{7-11} (below the coefficient F_7 is obtained by substituting $i = 1$, and so on, i.e., $F_8 \leftrightarrow i = 2$, ...):

$$\begin{aligned} F_i &= \int_0^1 du \left[C_5^i \delta_2 - C_6^i \frac{1}{t^2} \right] C_7^i, \\ \delta_2 &= \frac{2}{\sqrt{t^2 C}} \tanh^{-1} \left[\left(\frac{t^2}{C} \right)^{1/2} \right], \quad C_5^i = \frac{C}{t^2} B_{1,3}^i + B_{4,5}^i, \\ C_6^i &= 2B_{1,3}^i, \quad C_7^i = \{1, u, u^2, 1, u\}, \end{aligned} \quad (\text{B10})$$

where $C = m_e^2 - up'^2 - (1-u)p^2 + t_0^2$. For $F_{12} - F_{21}$ (below $F_{12} \leftrightarrow i = 1$):

$$\begin{aligned} F_i &= \int_0^1 dsdu \left[C_8^i \delta_3 + C_9^i \delta_4 \right] C_{10}^i, \\ \delta_3 &= \frac{1}{s(t^2)^2} \left\{ \left(\frac{B}{st^2} \right)^{1/2} \tanh^{-1} \left[\left(\frac{st^2}{B} \right)^{1/2} \right] - 1 \right\}, \quad \delta_4 = \frac{1}{t^2(B - st^2)}, \\ C_8^i &= -3B_{1,7}^i + 2t^2 B_{8,10}^i, \quad C_9^i = B_{1,7}^i, \\ C_{10}^i &= \{1, u, u^2, s, su, su^2, su^3, 1, s, su\}, \end{aligned} \quad (\text{B11})$$

where $B = m_e^2 - up'^2 - (1-u)p^2 + st_0^2$. And, finally, F_{22} is given by

$$F_{22} = \int_0^1 du \ln(u^2 k^2 / m_e^2 - uk^2 / m_e^2 + 1). \quad (\text{B12})$$

Appendix C: Many-potential term

Reduced matrix elements of the operators $I_F(\omega, \mathbf{r}_1, \mathbf{r}_2)$ and $I_C(\omega, \mathbf{r}_1, \mathbf{r}_2)$ can be derived using the PW expansion of the photon propagator. Namely, for this aim one needs the standard expansion formulas [84] for the functions which depend on r_{12} , such as

$$\frac{e^{i\omega r_{12}}}{r_{12}} = 4\pi i\omega \sum_{L=0}^{\infty} \sum_{M=-L}^L j_L(\omega r_{<}) h_L^{(1)}(\omega r_{>}) Y_{LM}^*(\hat{\mathbf{r}}_1) Y_{LM}(\hat{\mathbf{r}}_2). \quad (\text{C1})$$

Here, j_L and $h_L^{(1)}$ are the spherical Bessel function and spherical Hankel functions of the first kind, respectively and $r_{>} = \max(r_1, r_2)$ and $r_{<} = \min(r_1, r_2)$. Applying these formulas and performing the integrations over the angular variables, after some tedious manipulations one can obtain

$$\begin{aligned} \langle ab || I_F(\omega) || cd \rangle_J &= \alpha \int_0^\infty dr_1 r_1^2 \int_0^\infty dr_2 r_2^2 \left\{ (-1)^J G_J(\kappa_a, \kappa_c) G_J(\kappa_b, \kappa_d) g_J(\hat{\omega}, r_1, r_2) A_{ac}(r_1) A_{bd}(r_2) \right. \\ &\quad \left. + \sum_L (-1)^{L+1} [J] g_L(\hat{\omega}, r_1, r_2) D_{ac}^{JL}(r_1) D_{bd}^{JL}(r_2) \right\} \end{aligned} \quad (\text{C2})$$

for the Feynman gauge, and

$$\begin{aligned} \langle ab || I_C(\omega) || cd \rangle_J &= \alpha \int_0^\infty dr_1 r_1^2 \int_0^\infty dr_2 r_2^2 \left\{ (-1)^J G_J(\kappa_a, \kappa_c) G_J(\kappa_b, \kappa_d) \bar{g}_J(0, r_1, r_2) A_{ac}(r_1) A_{bd}(r_2) \right. \\ &\quad \left. + \sum_L (-1)^{L+1} a_{JL} g_L(\hat{\omega}, r_1, r_2) D_{ac}^{JL}(r_1) D_{bd}^{JL}(r_2) \right. \\ &\quad \left. + (-1)^{J+1} b_J [g_J^{\text{ret}}(\hat{\omega}, r_1, r_2) D_{ac}^{JJ+1}(r_1) D_{bd}^{JJ-1}(r_2) + g_J^{\text{ret}}(\hat{\omega}, r_2, r_1) D_{ac}^{JJ-1}(r_1) D_{bd}^{JJ+1}(r_2)] \right\} \end{aligned} \quad (\text{C3})$$

for the Coulomb gauge. In the above expressions, $[J] = 2J + 1$ and the following functions are defined:

$$g_J(\omega, r_1, r_2) = i[J] \omega j_{J,J}(\omega r_<) h_J^{(1)}(\omega r_>), \quad (\text{C4})$$

$$g_J(0, r_1, r_2) = \frac{r_<^J}{r_<^{J+1}}, \quad (\text{C5})$$

$$g_J^{\text{ret}}(\omega, r_1, r_2) = \begin{cases} i[J] \omega j_{J+1}(\omega r_1) h_{J-1}^{(1)}(\omega r_2), & \text{for } r_1 < r_2, \\ i[J] \omega j_{J-1}(\omega r_2) h_{J+1}^{(1)}(\omega r_1) - \frac{[J]^2 r_2^{J-1}}{\omega^2 r_1^{J+2}}, & \text{otherwise,} \end{cases} \quad (\text{C6})$$

The expressions depending on the radial wave functions read as

$$A_{ab}(r) = g_a(r) g_b(r) + f_a(r) f_b(r), \quad (\text{C7})$$

$$D_{ab}^{JL}(r) = g_a(r) f_b(r) H_L^J(\kappa_a, -\kappa_b) - f_a(r) g_b(r) H_L^J(-\kappa_a, \kappa_b). \quad (\text{C8})$$

Finally, the angular coefficients are

$$G_J(\kappa_a, \kappa_b) = (-1)^{j_b+1/2} \sqrt{[j_a][j_b][l_a][l_b]} \begin{pmatrix} l_a & J & l_b \\ 0 & 0 & 0 \end{pmatrix} \begin{Bmatrix} j_a & J & j_b \\ l_b & \frac{1}{2} & l_a \end{Bmatrix}, \quad (\text{C9})$$

$$H_L^J(\kappa_a, \kappa_b) = (-1)^{l_a} \sqrt{6[j_a][j_b][l_a][l_b]} \begin{pmatrix} l_a & L & l_b \\ 0 & 0 & 0 \end{pmatrix} \begin{Bmatrix} j_a & \frac{1}{2} & l_a \\ J & 1 & L \\ j_b & \frac{1}{2} & l_b \end{Bmatrix}, \quad (\text{C10})$$

$$a_{JL} = \begin{cases} J+1, & \text{for } L = J-1, \\ 2J+1, & \text{for } L = J, \\ J, & \text{for } L = J+1, \end{cases} \quad (\text{C11})$$

$$b_J = \sqrt{J(J+1)} \frac{\sqrt{[J+1][J-1]}}{[J]}. \quad (\text{C12})$$

Note that (C3) is consistent with Ref. [85], except for the typo in Eq. (B6) there.

Appendix D: Derivative of the free-electron self-energy operator

Let us represent the second derivative of the function $\Sigma_R^{(0)}$ with respect to the time component of the four-vector \mathbf{p} in the form:

$$\frac{\partial^2 \Sigma_R^{(0)}(\mathbf{p})}{\partial p_0^2} \Big|_{p_0=\varepsilon_a} = \frac{\alpha}{4\pi} \{ (N_1 + N_2 \gamma^0 - N_3 (\boldsymbol{\gamma} \cdot \mathbf{p})) \}, \quad (\text{D1})$$

where the coefficients N_1 , N_2 , and N_3 can be obtained by differentiating the formula (A6):

$$\begin{aligned} N_1 &= \frac{\partial^2 a(p_0, p)}{\partial p_0^2} \Big|_{p_0=\varepsilon_a}, \\ N_2 &= \varepsilon_a \frac{\partial^2 b(p_0, p)}{\partial p_0^2} \Big|_{p_0=\varepsilon_a} + \frac{\partial b(p_0, p)}{\partial p_0} \Big|_{p_0=\varepsilon_a} + \frac{\partial^2 c(p_0, p)}{\partial p_0^2} \Big|_{p_0=\varepsilon_a}, \\ N_3 &= \frac{\partial^2 b(p_0, p)}{\partial p_0^2} \Big|_{p_0=\varepsilon_a}. \end{aligned} \quad (\text{D2})$$

In the Feynman gauge, the derivatives of the coefficients a and b are (see [73, 75]):

$$\frac{\partial^2 a(p_0, p)}{\partial p_0^2} = -\frac{8}{m_e(1-\rho)} \left\{ 1 + \frac{1}{1-\rho} \left[\ln \rho - \frac{2p_0^2}{m_e^2} \left(\frac{1+\rho}{\rho} + \frac{2}{1-\rho} \ln \rho \right) \right] \right\}, \quad (\text{D3})$$

$$\frac{\partial b(p_0, p)}{\partial p_0} = \frac{2p_0}{m_e^2(1-\rho)^2} \left\{ 3 - \rho + \frac{2}{1-\rho} \ln \rho \right\}, \quad (\text{D4})$$

$$\frac{\partial^2 b(p_0, p)}{\partial p_0^2} = \frac{2}{m_e^2(1-\rho)^2} \left\{ 3 - \rho + \frac{2}{1-\rho} \left[\ln \rho - \frac{p_0^2}{m_e^2} \left(\frac{2+5\rho-\rho^2}{\rho} + \frac{6}{1-\rho} \ln \rho \right) \right] \right\}. \quad (\text{D5})$$

In the Coulomb gauge, it is more convenient to differentiate the free-electron self-energy operator in the form (A8):

$$\begin{aligned} \frac{\partial^2 \Sigma_R^{(0)}(\mathbf{p})}{\partial p_0^2} &= \frac{\alpha}{4\pi} \left\{ 2 \int_0^1 dx \left(\frac{\partial^2 \ln Y}{\partial p_0^2} [(1-x)\not{p} - m_e] + 2 \frac{\partial \ln Y}{\partial p_0} (1-x)\gamma^0 \right) + \right. \\ &\quad \left. + 2(\boldsymbol{\gamma} \cdot \mathbf{p}) \int_0^1 dx du \sqrt{x} \frac{\partial^2 \ln Z}{\partial p_0^2} \right\}. \end{aligned} \quad (\text{D6})$$

Then, for the coefficients $N_1 - N_3$ we have:

$$\begin{aligned} N_1 &= -2m_e \int_0^1 dx \frac{\partial^2 \ln Y}{\partial p_0^2} \Big|_{p_0=\varepsilon_a}, \\ N_2 &= 2 \int_0^1 dx (1-x) \left(\varepsilon_a \frac{\partial^2 \ln Y}{\partial p_0^2} \Big|_{p_0=\varepsilon_a} + 2 \frac{\partial \ln Y}{\partial p_0} \Big|_{p_0=\varepsilon_a} \right), \\ N_3 &= 2 \int_0^1 dx \left((1-x) \frac{\partial^2 \ln Y}{\partial p_0^2} \Big|_{p_0=\varepsilon_a} - \sqrt{x} \int_0^1 du \frac{\partial^2 \ln Z}{\partial p_0^2} \Big|_{p_0=\varepsilon_a} \right), \end{aligned} \quad (\text{D7})$$

where

$$\begin{aligned} \frac{\partial \ln Y}{\partial p_0} &= \frac{2p_0(x-1)}{m_e^2 - (p_0^2 - p^2)(1-x) - i0}, \\ \frac{\partial^2 \ln Y}{\partial p_0^2} &= \frac{2(x-1)(m_e^2 + (p_0^2 + p^2)(1-x))}{(m_e^2 - (p_0^2 - p^2)(1-x) - i0)^2}, \\ \frac{\partial^2 \ln Z}{\partial p_0^2} &= \frac{2(u-1)(m_e^2 + p_0^2(1-u) + p^2(1-xu))}{(m_e^2 - p_0^2(1-u) + p^2(1-xu) - i0)^2}. \end{aligned} \quad (\text{D8})$$

For the coefficient Z , the second derivative can be integrated analytically with respect to u :

$$\begin{aligned} \int_0^1 du \left(\frac{\partial^2 \ln Z}{\partial p_0^2} \right) &= 2 \left[\frac{p_0^4 - 3p_0^2(m_e^2 + p^2) - xp^2(m_e^2 + p^2 - 3p_0^2)}{m_e^2 \rho (p_0^2 - xp^2)^2} \right. \\ &\quad \left. - \frac{(m_e^2 + p^2(1-x))(3p_0^2 + xp^2)}{(p_0^2 - xp^2)^3} \ln \left(\frac{m_e^2 + p^2 - p_0^2}{m_e^2 + p^2(1-x)} \right) \right]. \end{aligned} \quad (\text{D9})$$

Some integrals over x from the expressions (D7) can be evaluated analytically using the following master integrals:

$$\begin{aligned} \int_0^1 dy \frac{y}{(m_e^2 - (p_0^2 - p^2)y)^2} &= \frac{1}{p_0^2 - p^2} \left(\frac{\ln \rho}{p_0^2 - p^2} + \frac{1}{m_e^2 \rho} \right), \\ \int_0^1 dy \frac{y^2}{(m_e^2 - (p_0^2 - p^2)y)^2} &= \frac{m_e^2}{(p_0^2 - p^2)^3} \left(\frac{1}{\rho} + 2 \ln \rho - \rho \right), \\ \int_0^1 dy \frac{y^3}{(m_e^2 - (p_0^2 - p^2)y)^2} &= \frac{1}{(p_0^2 - p^2)^4} (p_0^4 - 2(p_0^2 + 2m_e^2)p^2 + \frac{2m_e^4}{\rho} + 6m_e^4 \ln \rho \\ &\quad + 4m_e^2 p_0^2 + (p^2)^2 - 2m_e^4), \\ \int_0^1 dy \frac{y^2}{m_e^2 - (p_0^2 - p^2)y} &= -\frac{1}{2} \left(\frac{1}{p_0^2 - p^2} + \frac{2m_e^2}{(p_0^2 - p^2)^2} + \frac{2m_e^4 \ln \rho}{(p_0^2 - p^2)^3} \right). \end{aligned} \quad (\text{D10})$$